Chem Soc Rev

REVIEW ARTICLE

View Article Online
View Journal | View Issue

Cite this: *Chem. Soc. Rev.*, 2019, **48**, 285

Silicon oxides: a promising family of anode materials for lithium-ion batteries

Zhenhui Liu,†[a] Qiang Yu,†[a] Yunlong Zhao,[bcd] Ruhan He,[a] Ming Xu,[a] Shihao Feng,[a] Shidong Li,[a] Liang Zhou *[a] and Liqiang Mai *[a]

Received 4th August 2018

DOI: 10.1039/c8cs00441b

rsc.li/chem-soc-rev

Silicon oxides have been recognized as a promising family of anode materials for high-energy lithium-ion batteries (LIBs) owing to their abundant reserve, low cost, environmental friendliness, easy synthesis, and high theoretical capacity. However, the extended application of silicon oxides is severely hampered by the intrinsically low conductivity, large volume change, and low initial coulombic efficiency. Significant efforts have been dedicated to tackling these challenges towards practical applications. This Review focuses on the recent advances in the synthesis and lithium storage properties of silicon oxide-based anode materials. To present the progress in a systematic manner, this review is categorized as follows: (i) SiO-based anode materials, (ii) SiO_2-based anode materials, (iii) non-stoichiometric SiO_x-based anode materials, and (iv) Si–O–C-based anode materials. Finally, future outlook and our personal perspectives on silicon oxide-based anode materials are presented.

1. Introduction

With high energy density, long lifespan, and environmental friendliness, lithium-ion batteries (LIBs) represent one of the most attractive energy storage devices and are playing more and more important roles in modern society.[1–9] They have already conquered the markets of portable electronics, such as cell phones, laptops, and digital cameras. They have also been identified as the power sources of choice for electric vehicles and stationary energy storage. However, the current state-of-the-art LIBs cannot satisfy the ever-increasing demands of electric vehicles and large-scale energy storage.

Up to now, most commercialized LIBs have adopted intercalation reaction-based anode materials, such as graphite and $Li_4Ti_5O_{12}$. Such anode materials share the common features of outstanding cycle life but limited capacity. The theoretical capacities for graphite and $Li_4Ti_5O_{12}$ are 372 and 175 mA h g^{-1}, respectively.[10,11] The relatively low capacity severely limits the energy density of the batteries. Although anode materials based on alloying/de-alloying and conversion reactions, such as P (2596 mA h g^{-1}),[12,13] Sn (960 mA h g^{-1}),[7,14,15] Sb (660 mA h g^{-1}),[16,17] Ge (1600 mA h g^{-1}),[18–22] and transition

[a] *State Key Laboratory of Advanced Technology for Materials Synthesis and Processing, Wuhan University of Technology, Wuhan 430070, P. R. China. E-mail: liangzhou@whut.edu.cn, mlq518@whut.edu.cn*
[b] *Department of Chemistry and Chemical Biology, Harvard University, Cambridge, MA 02138, USA*
[c] *Advanced Technology Institute, University of Surrey, Guildford GU2 7XH, UK*
[d] *National Physical Laboratory, Teddington TW11 0LW, UK*
† These authors contributed equally to this work.

Zhenhui Liu

Zhenhui Liu received his BS degree from the Department of Applied Chemistry, Wuhan University of Technology in 2014 and he is currently working toward his PhD degree in Materials Science at Wuhan University of Technology. His current research involves nanomaterials and devices for energy storage.

Qiang Yu

Qiang Yu obtained his Bachelor's degree in 2015 from the School of Materials Science and Engineering, Liaocheng University. He is now a PhD candidate at Wuhan University of Technology with Prof. Liqiang Mai and Prof. Dongyuan Zhao. His research interests focus on the development of nanostructured carbon materials for application in supercapacitors and lithium-ion batteries.

metal oxides (TMOs)[23–25] are considered as promising alternative high-capacity candidates, none of them reached large-scale commercialization.

Among the emerging anode materials proposed for LIBs, Si has been considered as the most promising candidate to replace graphite. It is the second most abundant element in the earth's crust, environmentally friendly, and possesses an ultra-high theoretical capacity (4200 mA h g^{-1}).[26–28] However, the drastic volume fluctuation of Si (~400%) during lithiation/de-lithiation and the high production cost of nanostructured Si seriously hinder the widespread application.[6,29–32] Recently, silicon oxides have been considered as promising substitutes for elemental Si because of their extremely abundant reserves, low cost, and easy synthesis. In addition, silicon oxides show a small volume change during cycling when compared to elemental Si. The *in situ* generated Li_2O and lithium silicates during the first lithiation may buffer the large volume change and lead to improved cycling stability. Despite these merits, silicon oxides also suffer from several drawbacks, hindering their extensive application. (I) Silicon oxides are insulators with low intrinsic electrical conductivity, which lowers the electrochemical activity. (II) Although the volume change issue is not as serious as that in elemental Si, it is non-negligible. (III) The initial coulombic efficiency (ICE) of silicon oxides is relatively low, which is associated with the irreversible formation of Li_2O and lithium silicates in the first cycle.

Recently, significant efforts have been devoted to tackling the above-mentioned issues and pushing the silicon oxide-based anode materials towards practical applications in LIBs.[33] Actually, silicon oxides have been blended with graphite (usually with a content of less than 10%) and used in commercialized LIBs.[2,34] Up to now, there have been several excellent reviews on Si-based anode materials;[35–37] however, a comprehensive review exclusively focusing on silicon oxide-based anode materials is lacking. This Review summarizes the most recent advances in the microstructure, lithium storage mechanisms, rational synthesis, and electrochemical properties of silicon oxide-based anode materials. To present the results in a systematic manner, this review is categorized as follows: (i) SiO-based anode materials, (ii) SiO_2-based anode materials, (iii) non-stoichiometric SiO_x-based anode materials, and (iv) Si–O–C-based anode materials. At the end of this Review, our personal perspectives on silicon oxide-based anode materials are presented.

2. SiO-based anode materials

Among the various silicon oxides (SiO, SiO_2, SiO_x, and Si–O–C), SiO has attracted the most attention as the anode materials for LIBs. It was first reported in 1887 by Charles F. Mabery.[38] Commercially available SiO is usually produced by heating SiO_2 and Si mixtures at elevated temperatures to generate gaseous SiO (SiO_2 + Si = 2SiO) and then condensing the SiO vapor.[39]

2.1 The atomic structure of amorphous SiO

The atomic structure of SiO has been a subject of controversy since its discovery.[40,41] Philipp proposed a random-bonding model, which described the SiO as a homogeneous single-phase material with a continuous Si–(O_xSi_{4-x}) network composed of randomly distributed Si–Si and Si–O bonds.[42,43] Brady[44] and Temkin[45] suggested a random-mixture model, in which the SiO was described as a mixture of nanosized amorphous Si and SiO_2. More realistic models suggested that silicon suboxide may exist in the interfacial regions between Si and SiO_2 domains.[46–48] The interface boundary layer accounts for 20–25% of the total number of atoms in SiO.[48]

Due to the limitation in spatial resolution of conventional characterization techniques, the direct experimental observation of the local atomic structure of SiO is very challenging. Very recently, Chen and co-workers provided experimental evidence on the atomic-scale disproportion of amorphous SiO. Using angstrom-beam electron diffraction (ABED), they detected silicon suboxide-type tetrahedral coordinates at the Si/SiO_2 boundaries.[49] Based on the ABED and synchrotron X-ray scattering results as well

Liang Zhou

Liang Zhou received his BS (2006) and PhD (2011) from Fudan University (with Prof. Dongyuan Zhao and Prof. Chengzhong Yu). He then carried out postdoctoral research in Prof. Xiong Wen (David) Lou's group at Nanyang Technological University and Prof. Chengzhong Yu's group at The University of Queensland. He is currently a Professor at Wuhan University of Technology. His research interests focus on functional nanomaterials for energy storage and conversion applications.

Liqiang Mai

Liqiang Mai received his PhD degree from Wuhan University of Technology in 2004. He then carried out postdoctoral research in Prof. Zhonglin Wang's group at Georgia Institute of Technology (2006–2007) and worked as an advanced research scholar in Prof. Charles M. Lieber's group at Harvard University (2008–2011). He is currently a Chair Professor at Wuhan University of Technology. His research interests include nanowires, micro-/nano-energy-storage devices, and energy-based nano-bio interfaces.

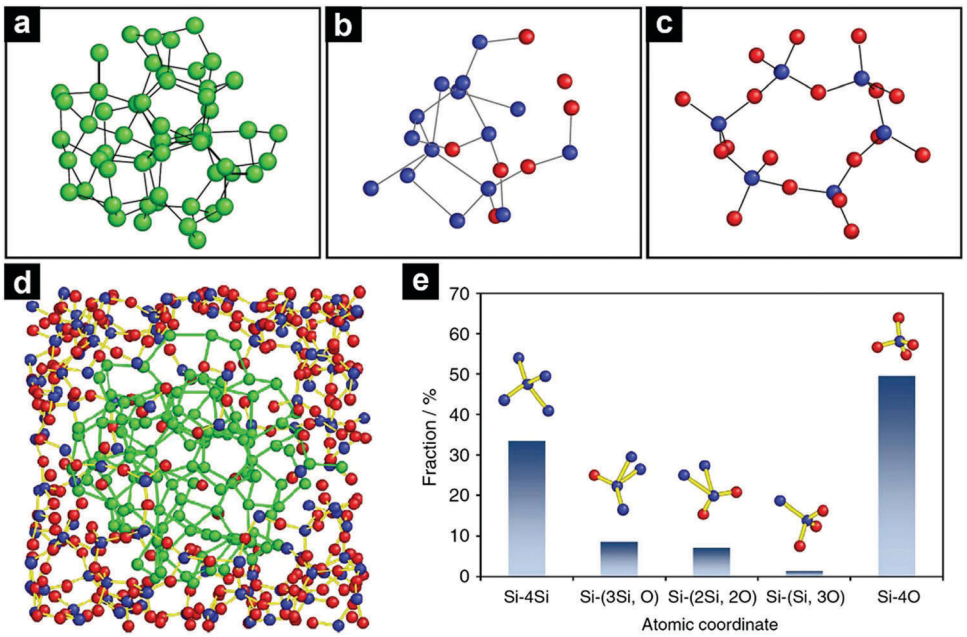

Fig. 1 Atomic models of amorphous Si (a), interfacial silicon suboxide (b), and amorphous SiO_2 (c). The model of amorphous SiO (d). Fractions of the five atomic coordinates existing in amorphous SiO (e). The $Si–Si_4$ is from the Si clusters; the $Si–O_4$ is from the SiO_2 matrix; the $Si–(Si_3O)$, $Si–(Si_2O_2)$, and $Si–(SiO_3)$ are from the Si/SiO_2 interfaces. Reproduced with permission from ref. 49. Copyright 2016, Nature Publishing Group.

as computer simulations, the model of disproportionated SiO was proposed (Fig. 1).

Due to the inhomogeneous nature (disproportion) on the atomic-scale, SiO is thermodynamically unstable and it tends to disproportionate to Si and SiO_2 ($2SiO \rightarrow Si + SiO_2$).[50–52] Considering this fact, the Si/SiO_2-based composites derived from disproportionated SiO are denoted as d-SiO in this Review.

2.2 Lithiation behavior of SiO

To the best of our knowledge, the utilization of SiO in LIBs was first reported in the 1990s.[53–55] In 2001, Tatsumisago *et al.* reported the lithium storage performances of amorphous SiO/SnO (50/50 mol%) prepared by mechanical milling of SiO and SnO.[56] A high reversible capacity of ~800 mA h g^{-1} was obtained for the SiO/SnO composite. In 2002, Yang and co-workers examined a series of SiO_x with different O contents (SiO, $SiO_{0.8}$, $SiO_{1.1}$) and found that the capacity dropped with the increase of O content.[57] On the other hand, the increased O content (decreased capacity) alleviated the volume change and thus improved the cycling performance. $SiO_{0.8}$ demonstrated a reversible capacity of ~1600 mA h g^{-1}. These pioneering works inspire scientists' interests in SiO-based anode materials.[58–66]

Understanding the lithiation/de-lithiation mechanisms is of vital importance to further improve the electrochemical performance of SiO.[67–77] It is generally accepted that Li_xSi alloys, lithium silicates (Li_4SiO_4, $Li_2Si_2O_5$, $Li_6Si_2O_7$, Li_2SiO_3), and Li_2O are formed during the first lithiation of SiO. The extraction/insertion of Li^+ in Li_xSi alloys is reversible. Assuming all the Si in SiO can be converted into $Li_{4.4}Si$ during lithiation, the theoretical reversible capacity of SiO reaches 2680 mA h g^{-1}. The lithium silicates and Li_2O are generally irreversible phases. On the one hand, they serve as a buffering matrix against the volume change during lithiation/de-lithiation, enhancing the cycling performance of SiO.[68,78] On the other hand, the formation of irreversible lithium silicates and Li_2O lowers the ICE of SiO.[68,70,75]

The composition of the lithiated products of SiO is relatively complex. Various lithium silicates have been observed in the lithiated SiO and they behave quite differently depending on the compositions. Sohn *et al.* identified three lithium silicate species ($Li_2Si_2O_5$, Li_4SiO_4 and $Li_6Si_2O_7$) in the discharge products of SiO. Among these phases, only the $Li_2Si_2O_5$ phase was demonstrated to be reversible, whereas the Li_4SiO_4 and $Li_6Si_2O_7$ were irreversible during cycling.[74,76] To understand the kinetics of the lithiated products of SiO, Yoon *et al.* controlled the amount of Li^+ insertion ("mole control") at various C-rates.[75] It is found that the irreversible capacity increased with mole rate but decreased with C-rates. This study suggests that the composition of the discharged products is related to the depth of discharge and C-rate.

The lithiation process of SiO was studied by Han *et al.* through first-principles molecular dynamics simulations. The calculations revealed that lithium silicates were dominant over Li_2O as irreversible matrix components of the lithiated SiO ($Li_{4.4}SiO$).[77] Although Li_2O had a minor portion in the lithiated SiO, the Li^+ diffusivity in Li_2O was at least two orders of magnitude higher than those in lithium silicates. As a result, it could act as the main Li^+ transport channel to access the Li_xSi core, maximizing the capacity and rate capability of SiO. This study provides the possibility of boosting the electrochemical performances of SiO-based anode materials *via* controlling the inactive matrix components.

Based on the above studies, the lithium storage mechanism of SiO can be proposed as follows:

$$SiO + 2Li^+ + 2e^- \rightarrow Si + Li_2O \quad (1)$$

$$4SiO + 4Li^+ + 4e^- \rightarrow 3Si + Li_4SiO_4 \quad (2)$$

$$5SiO + 2Li^+ + 2e^- \rightarrow 3Si + Li_2Si_2O_5 \quad (3)$$

$$7SiO + 6Li^+ + 6e^- \rightarrow 5Si + Li_6Si_2O_7 \quad (4)$$

$$3SiO + 2Li^+ + 2e^- \rightarrow 2Si + Li_2SiO_3 \quad (5)$$

$$Si + xLi^+ + xe^- \leftrightarrow Li_xSi \quad (6)$$

2.3 Electrochemical performances of SiO

Due to the existence of lithium silicates and Li_2O, the volume variation of SiO during lithiation/de-lithiation is significantly reduced and the cycling stability is enhanced when compared to Si. However, complete elimination of the volume change issue is difficult. According to recent literature studies, the volume expansion of SiO is around 200% upon lithiation.[68,79,80] Such a drastic volume expansion may induce stress in the active materials, resulting in active material pulverization and isolation, electrode disintegration, high surface side reactions, as well as repetitive solid electrolyte interface (SEI) film formation and rupture.[81] Therefore, the large volume change of SiO is considered to be the main reason for its capacity fading upon cycling. Besides, SiO also suffers from low ICE and low rate capability. The former originates from the formation of irreversible lithium silicates and Li_2O during the first cycle, whereas the latter is caused by low intrinsic electrical conductivity. For practical applications, there is still considerable room for improving the cyclability, ICE, and rate capability of SiO.

2.3.1 Bare SiO anode materials. Various strategies, such as downsizing,[72,74] constructing porous structures,[76] nano-compositing,[62,82,83] and employing new binders,[79,80,84,85] have been dedicated to tackling the volume change issue of SiO-based anodes. The commercially available SiO is usually micrometer-sized and shows a poor cycling performance. To reduce the particle size and broke the microstructure of SiO, Sohn *et al.* employed a high-energy mechanical milling (HEMM) process (Fig. 2a).[72] Combining the disproportionation reaction of SiO ($2SiO \rightarrow Si + SiO_2$) and HEMM, a d-SiO-based anode composed of nanosized Si embedded in a SiO_x matrix was obtained. The bare HEMM-treated d-SiO delivered a reversible capacity of $\sim$1000 mA h g^{-1} with good retention (Fig. 2b). By HEMM SiO followed by surface etching with NaOH, SiO with better electrochemical performances could be obtained.[74] The synthesized SiO provided a high capacity of 1260 mA h g^{-1} after 50 cycles and the capacity retention is 86.5% against the second cycle. The enhanced capacity and cyclability were ascribed to the reduced particle size and the removal of O-rich SiO_x on the surface, which would slow the Li^+ diffusion. Both studies indicate that even bare SiO may show good lithium storage performances provided that its microstructure and size are properly engineered.

Constructing porous structures has also been employed to boost the cycling stability of SiO. The porous structures provide

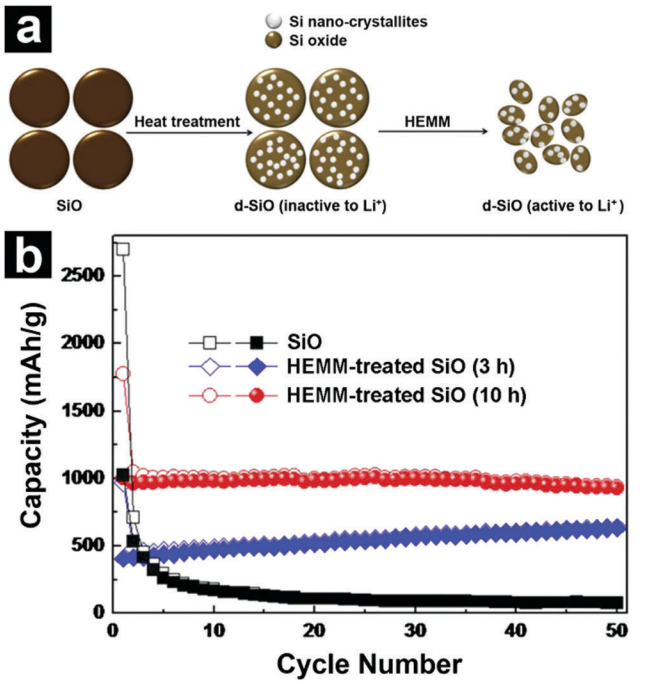

Fig. 2 Schematic illustration for the preparation of d-SiO (a). The synthesis of d-SiO includes two steps: disproportionation of SiO at 1200 °C and HEMM. Cycling performances of SiO (b), HEMM-treated d-SiO (3 h) and HEMM-treated d-SiO (10 h). Reproduced with permission from ref. 72. Copyright 2013, Elsevier Ltd.

not only free space for volume expansion accommodation but also efficient channels for Li^+ diffusion. As mentioned previously, the disproportionated SiO (d-SiO) is a composite material composed of nanocrystalline Si and an amorphous SiO_2 matrix. When subjected to NaOH solution, the nanocrystalline Si was attached by NaOH vigorously, while the SiO_2 matrix was etched away slowly. In this sense, the nanocrystalline Si acted as a pore generating agent, and porous SiO_x was obtained after NaOH etching (Fig. 3a–c).[76] The porous SiO_x without any carbon coating demonstrated a high capacity of $\sim$1240 mA h g^{-1} after 100 cycles (Fig. 3d). Due to the fast Li^+ diffusion in the pores, the porous SiO_x manifested excellent rate performance as well (Fig. 3e).

2.3.2 SiO/C hybrid anode materials. Among the various electrochemical performance optimization strategies, compositing SiO with conductive carbon has been most extensively studied. Various SiO/C composites have been constructed and assessed.[86–92] The carbon not only alleviates the overall volume change, but also improves the conductivity of SiO, leading to enhanced cycling stability and rate capability. Ohzuku's group reported a SiO/C composite composed of 50 wt% SiO, 21 wt% graphite, 9 wt% carbon fiber, and 20 wt% deposited carbon, which manifested a discharge capacity of 700 mA h g^{-1} after 100 cycles in laminate-type cells.[87] By coupling the SiO/C composite anode with a $LiCo_{1/3}Ni_{1/3}Mn_{1/3}O_2/LiCoO_2$ cathode, prototype 14 500 batteries were fabricated. The prototype 14 500 battery delivered a capacity of 1 A h at 200 mA with 70% capacity retention after 300 cycles.[93] Using chemical vapor deposition (CVD), Oh and co-workers prepared a micrometer-sized d-SiO/C composite (Fig. 4a).[89,90]

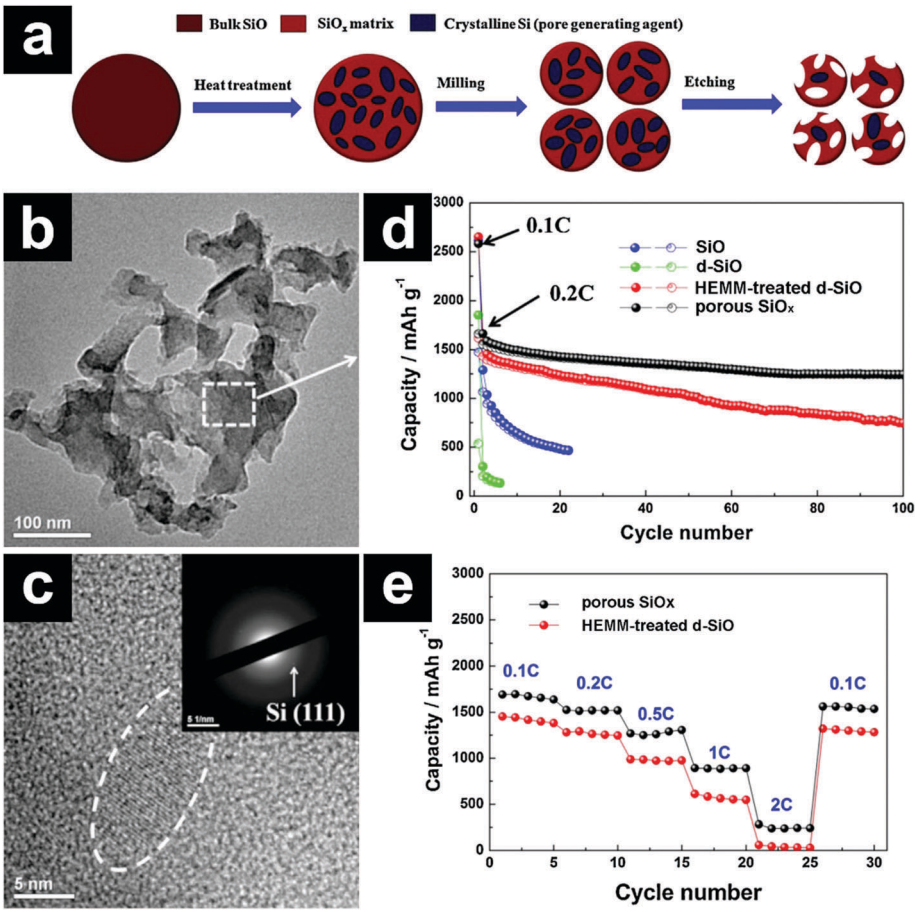

Fig. 3 Schematic illustration for the preparation of porous SiO_x (a); TEM (b) and HRTEM (c) images of porous SiO_x; cycling performances of SiO, d-SiO, HEMM-treated d-SiO, and porous SiO_x (d); rate performances of HEMM-treated d-SiO and porous SiO_x (e). 1C = 1500 mA h g^{-1}. The inset in e shows the SAED pattern of porous SiO_x. Reproduced with permission from ref. 76. Copyright 2014, Elsevier Ltd.

The d-SiO/C composite exhibited a high capacity fading attributed to the electric disconnection, limited buffering effect of lithium silicates, and crumbling of d-SiO/C. In another study, Choi and co-workers fabricated N-doped carbon coated d-SiO (d-SiO/NC) using N-containing ionic liquid as the carbon precursor.[91] The micrometer-sized NC–d-SiO manifested enhanced capacity and rate capability compared with the carbon coated d-SiO and bare d-SiO counterparts.

More recently, a fascinating vertical graphene coated micrometer-sized d-SiO (d-SiO@vG) anode was prepared through a CVD method by Liu and co-workers.[94] Due to the unique structure with stable electrical contacts, fluent Li^+ diffusion channels, and elastic buffering layer (Fig. 5a–c), the d-SiO@vG demonstrated a high specific capacity of 1600 mA h g^{-1} with excellent capacity retention (Fig. 5d). Full cells based on the d-SiO@vG/graphite (5% : 95%) anode and NCA cathode ($LiNi_{0.8}Co_{0.15}Al_{0.05}O_2$) were also assembled. With the addition of only 5 wt% d-SiO@vG, the energy density of the full cell was increased by 15% (Fig. 5e and f).

In most of the reports on SiO/C composite anodes, ball milling is combined with carbon coating to further enhance the performance.[62,82,83,95–97] For example, Morita and Takami

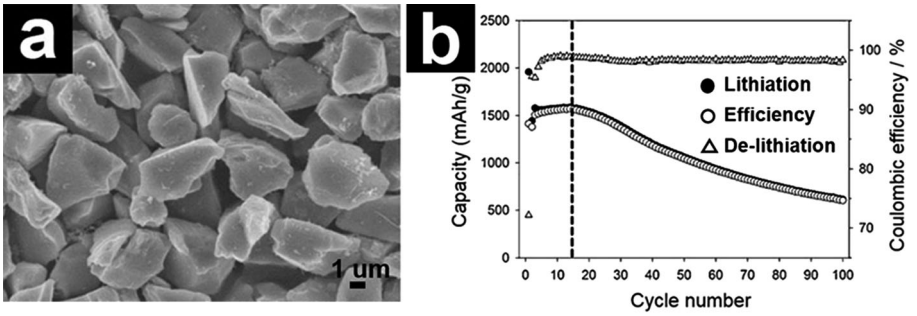

Fig. 4 SEM image of d-SiO/C (a) and cycling performance of d-SiO/C. (b) Reproduced with permission from ref. 90. Copyright 2013, Elsevier Ltd.

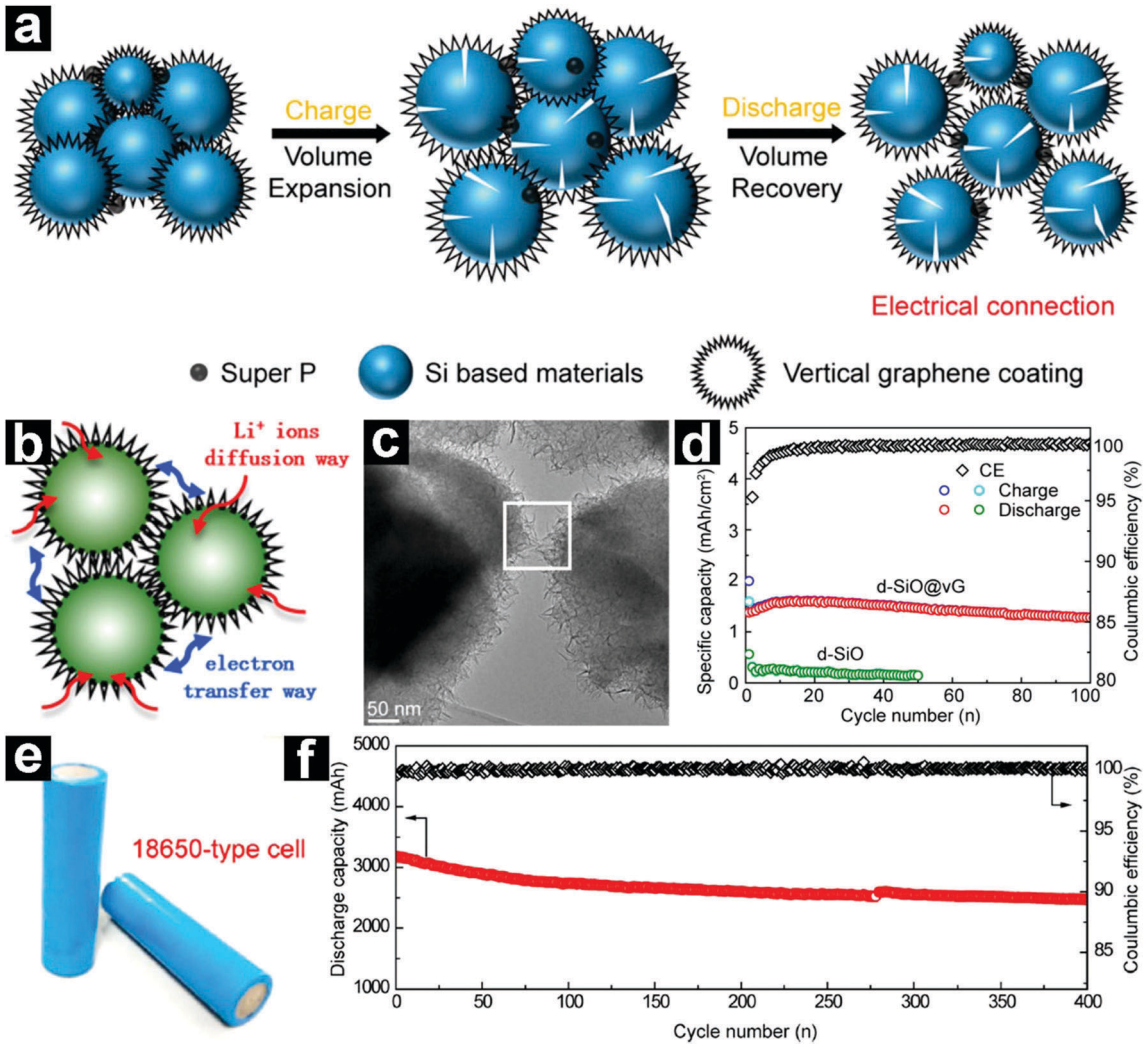

Fig. 5 Schematic illustration of the d-SiO@vG during charge/discharge (a); schematic structure (b) and TEM image (c) of d-SiO/vG; cycling performances of d-SiO and d-SiO@vG at 320 mA g^{-1} (d); digital photos of the assembled d-SiO@vG/graphite//NCA 18 650 full cells (e); cycling performance of the full cell (f). Reproduced with permission from ref. 94. Copyright 2017, American Chemical Society.

synthesized a Si/SiO_x/C nanocomposite (d-SiO/C) with a Si size of 5–10 nm by ball milling, furfuryl alcohol polymerization, and disproportionation of SiO.[62] The obtained Si/SiO_x/C nanocomposite (d-SiO/C) delivered a high reversible capacity of ~700 mA h g^{-1} for 200 cycles. Sohn *et al.* prepared a d-SiO/C composite by ball-milling and pyrolysis.[82] Polyvinyl alcohol (PVA) was used as the carbon precursor and the SiO was disproportionated into nanocrystalline Si and amorphous SiO_2.

The resultant d-SiO/C exhibited an ICE value of 76% and a capacity of 710 mA h g^{-1} after 100 cycles at 100 mA g^{-1}. A d-SiO/graphite composite was prepared by the same group; it demonstrated a first discharge capacity of 1002 mA h g^{-1}, retaining 710 mA h g^{-1} after 100 cycles.[95] A SiO/graphite composite anode was synthesized by Doh and co-workers through HEMM.[83] The SiO/graphite manifested a capacity of 688 mA h g^{-1} after 30 cycles. Takeda *et al.* fabricated a SiO/carbon nanofiber (SiO/CNF) anode using HEMM; the as-synthesized SiO/CNF provided a specific capacity of 724 mA h g^{-1} with excellent cycling performance for 200 cycles.[96]

The fabrication of porous structures with conductive carbon coating on the surface integrates the advantages of both strategies.[98–100] Lee and Park developed a metal-assisted chemical etching process for the fabrication of a three-dimensional (3D) porous SiO anode from bulk SiO.[99] Ag nanoparticles were first deposited on the surface of SiO through galvanic displacement (Fig. 6a). When the Ag/SiO was immersed in HF/H_2O_2, the SiO was continuously etched off through localized electrochemical processes, forming a 3D porous structure. After removal of the Ag nanoparticles with HNO_3, 3D porous SiO could be obtained. Coating the porous SiO with acetylene-derived carbon by CVD led to the formation of porous SiO/C (Fig. 6b). The porous SiO/C delivered a high capacity of 1490 mA h g^{-1} after 50 cycles at 0.1C (Fig. 6c). In addition, a capacity of 1130 mA h g^{-1} could be achieved at 3C.

The disproportionation of SiO into Si/SiO_2 usually takes place at relatively high temperatures (~1000 °C). The introduction of catalyst (NaOH) lowers the disproportionation temperature to ~700 °C (the so-called chemical-assisted thermal disproportionation). By combining metal-assisted chemical etching and

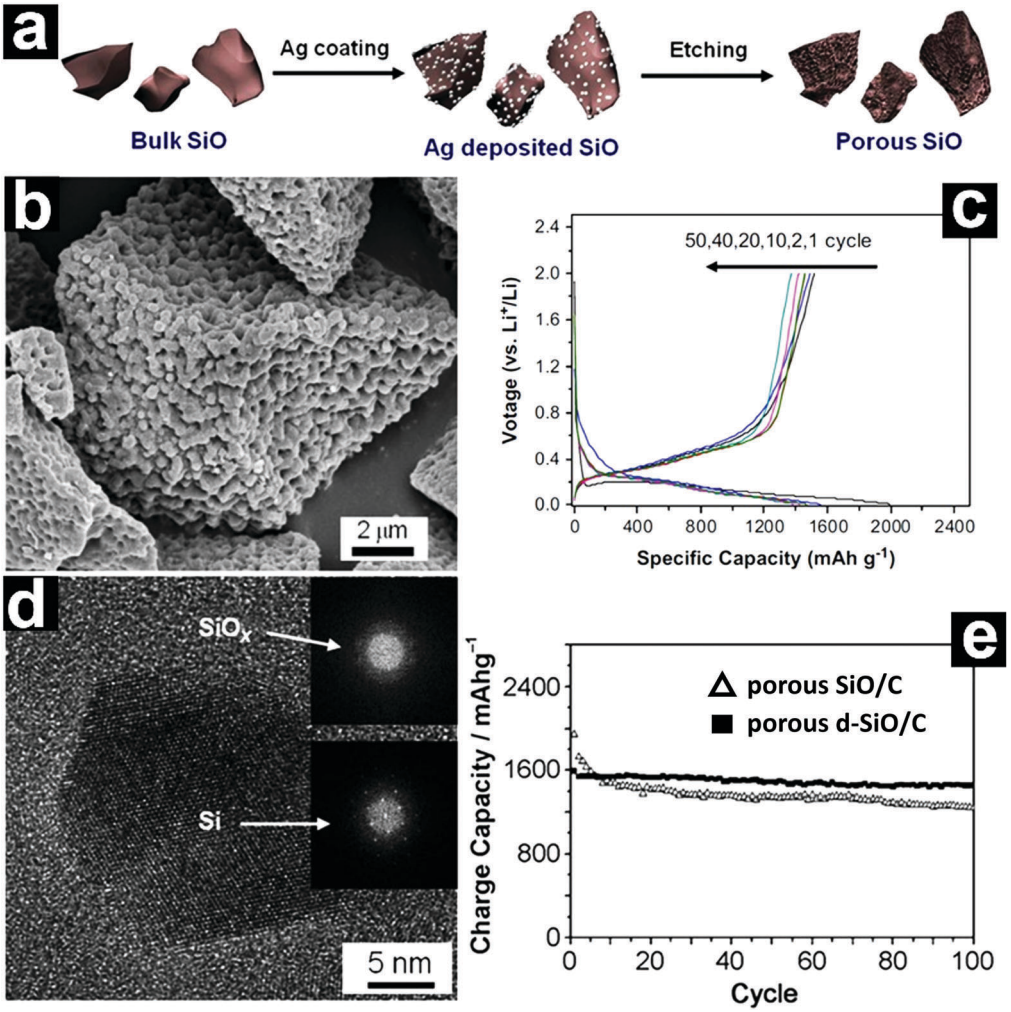

Fig. 6 Schematic illustration of the synthesis of porous SiO *via* metal-assisted etching (a); SEM image of porous SiO/C (b); discharge–charge profiles of porous SiO/C (c); HRTEM image of porous d-SiO showing the nanocrystalline Si/amorphous SiO_x composite structure (d); cycling performances of porous SiO/C and d-SiO/C (e). (a–c) Reproduced with permission from ref. 99. Copyright 2013, Elsevier Ltd. (d and e) Reproduced with permission from ref. 100. Copyright 2012, Wiley-VCH.

chemical-assisted thermal disproportionation, Park and co-workers prepared a porous multi-component Si/crystalline SiO_2/amorphous SiO_x (d-SiO) composite (Fig. 6d).[100] After coating with carbon, the porous d-SiO/C manifested excellent electrochemical performance, even better than that of porous SiO/C. A reversible capacity of $\sim$1600 mA h g^{-1} could be obtained at 0.1C, retaining 91.3% of the capacity after 100 cycles (Fig. 6e).

2.3.3 SiO/metal and SiO/metal oxide hybrid anode materials. Besides carbon, metals and metal oxides have also been used to composite with SiO to improve its lithium storage performance.[56,65,101–103] Early in 2001, Tatsumisago reported the synthesis of SiO/SnO composites by mechanical milling SiO and SnO in an inert atmosphere (Table 1).[56] By HEMM of SiO and Al, Kim *et al.* prepared a nanostructured $SiAl_{0.2}O$ anode composed of Si nanocrystals (<10 nm) embedded in amorphous aluminosilica.[65] The $SiAl_{0.2}O$ provided a high capacity of 800 mA h g^{-1} over 100 cycles. Jeong *et al.* reported a TiO_2 coated SiO composite anode by a sol–gel process. The TiO_2 coated SiO demonstrated higher specific capacity, higher ICE, better rate capability, as well as better cycling stability than the pristine SiO.[101] A Fe_2O_3 nanoparticle decorated SiO composite was prepared by mechanical milling by Wang *et al.*[103] The SiO/Fe_2O_3 composite exhibited enhanced lithium storage performances in terms of ICE (68%), rate capability (600 mA h g^{-1} at 4.8 A g^{-1}), and cyclability (71% capacity retention after 50 cycles) compared to bare SiO.

Amine and co-workers reported a novel family of composite anode materials, SiO/$Sn_xCo_yC_z$, by ultrahigh energy ball milling. The anode material composed of 50 wt% SiO and 50 wt% $Sn_{30}Co_{30}C_{40}$ delivered stable specific capacities of 1040 and 900 mA h g^{-1} at 100 and 300 mA g^{-1}, respectively.[104] A family of SiO/$Sn_xFe_yC_z$ materials was prepared by the same group as well. Fe was chosen to replace Co in the composite anode materials due to its low cost and environmental friendliness. The SiO/$Sn_{30}Fe_{30}C_{40}$ anode delivered specific capacities of 900 and 700 mA h g^{-1} at 300 and 800 mA g^{-1}, respectively.[105]

2.3.4 Optimizing the binder for SiO-based anode materials. Polymer binders have a great influence on the cyclability of SiO-based anodes as well. The high capacity of SiO is accompanied

Table 1 Electrochemical performances of SiO-based anode materials

Year	Sample	Initial discharge/charge capacity (mA h g^{-1})	ICE (%)	Cycling performance (mA h g^{-1})	Ref.
2001	SiO/SnO	~590/~293	43	340 (20 cycles)	56
2002	SiO	2600/1600	62	~810 (17)	57
2006	d-SiO/C	~1000/~700	~68	<700 (200 cycles)	62
2007	d-SiO/C	1050/800	76	710 (100 cycles)	82
2007	Li/SiO derived composite	951/770	81	762 (50 cycles)	63
2007	Ni doped SiO	1850/1556	84	—	78
2008	SiO/graphite	1556/693	45	688 (30 cycles)	86
2009	Li/SiO	1364/994	72.8	~860 (20 cycles)	109
2010	Li/SiO	989/1000	101.07	710 (20 cycles)	110
2010	d-SiO/graphite	1516/1002	66	710 (100 cycles)	95
2010	$SiAl_{0.2}O$	2240/1510	67.4	800 (100 cycles)	65
2011	SiO/C	1200/870	72.5	700 (100 cycles)	87
2011	SiO/CNF	2027/724	35.7	675 (200 cycles)	96
2012	d-SiO/C	1380/1307	94.7	578 (90 cycles)	89
2012	d-SiO/C	1930/1598	82.8	1459 (100 cycles)	100
2012	SiO/TiO_2	1757/1265	72	—	101
2012	$SiO/Sn_{30}Co_{30}C_{40}$	1480/1030	69.6	1040 (50 cycles)	104
2013	SiO/C	1990/1520	76.4	1490 (50 cycles)	99
2013	d-SiO/C	1958/1413	72.2	~600 (100 cycles)	90
2013	SiO	1779/1002	56.3	~1000 (50 cycles)	72
2013	SiO	2366/1467	62	1260 (50 cycles)	74
2013	d-SiO/NC	2024/1496	73.9	955 (200 cycles)	91
2013	SiO/Fe_2O_3	2773/1893	68	1335 (50 cycles)	103
2013	SiO/Fe_2SiO_4	2095/1900	89.3	~1000 (25 cycles)	113
2013	$SiO/Sn_{30}Fe_{30}C_{40}$	1427/961	67	538 (100 cycles)	105
2014	Porous SiO	2653/1709	64.4	1242 (100 cycles)	76
2016	Li/SiO	1220/1001	82.12	~750 (15 cycles)	111
2016	Pre-lithiated SiO	—	94.9	906 (100 cycles)	112
2017	d-SiO@vG	—	—	1600 (100 cycles)	94

by a large volume expansion of 200%, which causes the notorious problems of active material pulverization at the particle level and disintegration at the electrode level. Suitable binders can provide persistent contacts among the active materials, conductive carbons, and current collector, improving the electrode integrity effectively. Komaba *et al.* examined four types of polymer binders, including poly(acrylic acid) (PAA), PVA, sodium carboxymethyl cellulose (CMCNa), and conventional poly(vinylidene fluoride) (PVDF). They found PAA was the most suitable binder for the SiO anode (Fig. 7a).[79] The SiO-based electrode with PAA binder delivered a capacity over 700 mA h g^{-1} with excellent cycling stability (Fig. 7b). The improved cyclability was attributed to the strong interactions between –COOH groups and surface Si–OH groups as well as the uniform coating of amorphous PAA on SiO, which effectively held the fractured SiO particles and suppressed the loss of electrical isolation (Fig. 7c and d). By screening environmentally friendly aqueous binders for SiO/C, Yang *et al.* found that PAA, styrene butadiene rubber/sodium carboxymethyl cellulose (SCMC), and especially sodium alginate (Alg) led to much better lithium storage performance than PVA.[80] The SiO/C electrodes with Alg and SCMC binders led to a high specific capacity of 940 mA h g^{-1} after 100 cycles.

To achieve satisfactory cycling performances for high-capacity anode materials, larger amounts of binders and conductive carbons than those used in traditional electrodes are usually required. These inactive additives inevitably sacrifice the energy density of the batteries, making them less competitive. By employing a functional conductive polymer binder, poly(9,9-dioctylfluorene-*co*-fluorenone-*co*-methylbenzonic ester) (PFM), Liu *et al.* fabricated highly durable SiO-based electrodes with 98% micro-sized SiO/C, 2% PFM binder without any conductive carbons (Fig. 8a).[84] Such a novel binder enabled molecular-level electronic connections between active materials and the conductive polymer matrix by integrating adhesion and electrical conduction (Fig. 8b and c). The SiO/C electrode with PFM binder demonstrated a stable high reversible capacity (>1000 mA h g^{-1}) for 500 cycles with a capacity retention of over 90% (Fig. 8d). The areal capacity reached close to 2 mA h cm^{-2} (Fig. 8e). By calendering the electrode to optimize the porosity, the area capacity of the SiO-based electrode with PFM binder could be improved to ~3.5 mA h cm^{-2}.[85] By introducing a sacrificial agent, NaCl, in the electrode, the porosity of the electrode could be well controlled and the areal capacity of the electrode could be further increased to ~4 mA h cm^{-2}.[106]

2.3.5 ICE improvement for SiO-based anode materials. The large irreversible capacity during the initial cycle significantly hinders the practical application of SiO in LIBs. It necessitates an excess amount of cathode materials solely for the initial cycle, sacrificing the energy density of the full cell. Therefore, many efforts have been devoted to improving its ICE. For example, by HEMM SiO with Li, Wen *et al.* prepared a composite anode material composed of nanocrystalline Si, Li_4SiO_4, and other Li-rich components (Li_2O).[63] The obtained Li/SiO derived composite exhibited a first discharge capacity of 951 mA h g^{-1} with a high ICE of 81%. This method could be easily generalized to the construction of nanosized Si/Sn-based composite and Si-based glassy composite anodes.[107,108] Yoon *et al.* synthesized a pre-lithiated SiO/C anode, which demonstrated reduced initial capacity loss and enhanced ICE in comparison with the pristine SiO/C.[109] A SiO and Li powder double layer anode technique was

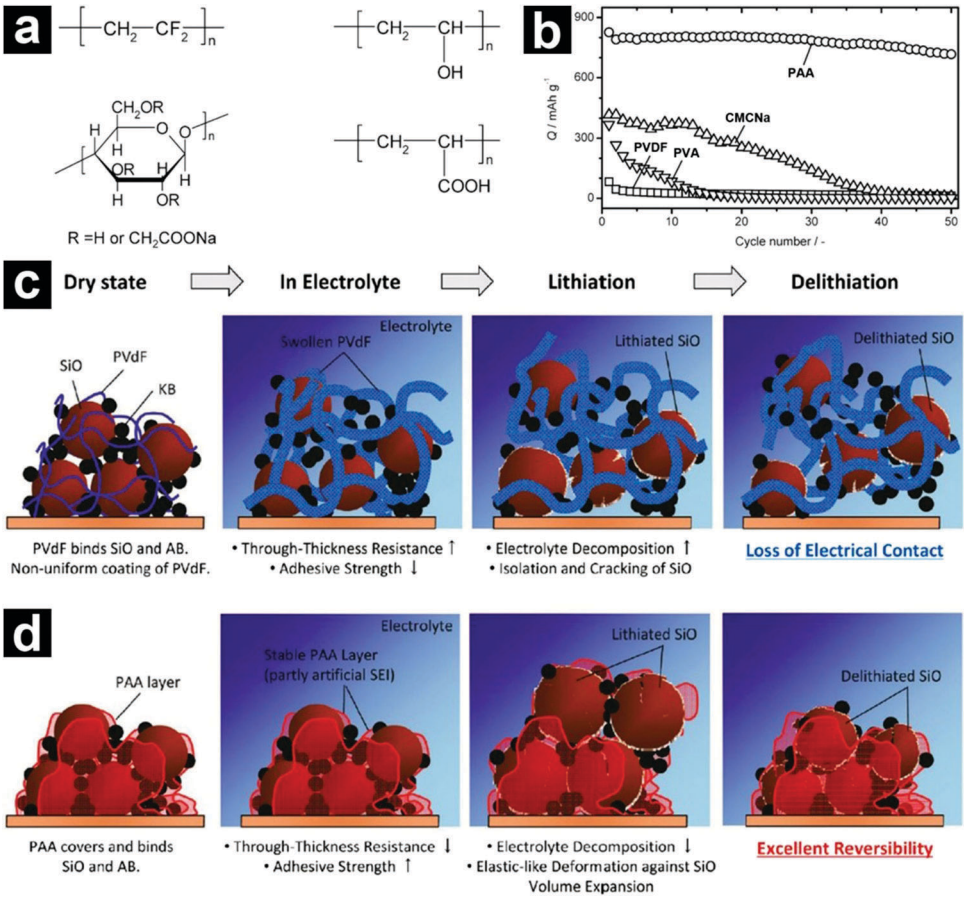

Fig. 7 Chemical structures of PVDF, PVA, CMCNa, and PAA binders (a). Cycling performances of SiO-based electrodes with different binders (b). Schematic illustration of the SiO-based electrodes with PVDF (c) and PAA (d) binders during charge/discharge. Reproduced with permission from ref. 79. Copyright 2011, American Chemical Society.

also developed by the same group, and an ICE value of over 100% was achieved.[110] By heating the SiO and Li mixture at high temperatures (600 °C), the ICE of SiO could also be increased.[111] The heated SiO and Li mixture with a weight ratio of 7 : 1 demonstrated an ICE value of 82.12%, much higher than that of pristine SiO (58.52%). It was found that irreversible phases, such as lithium silicates and Li_2O, were formed during the solid state reaction of SiO and Li, and the preformed irreversible phases prevented the consumption of Li^+ during the first cycle.

More recently, a scalable roll-to-roll pre-lithiation technology based on electrical shorting with Li was developed by Choi *et al.* (Fig. 9).[112] The degree of pre-lithiation could be finely tuned *via* controlling the accurate shorting time and voltage monitoring. With an optimized shorting time, the pre-lithiated SiO showed a high ICE value of 94.9%. When coupled with a NCA cathode, the full cell led to an energy density 1.5 times that of traditional graphite//$LiCoO_2$ counterparts based on the weight of active materials.

Interestingly, compositing SiO with metals or metal oxides could also improve the ICE of SiO to some extent. For example, Miyachi *et al.* synthesized Fe, Ni, and Ti doped SiO anodes, among which the Ni doped SiO (25 wt% Ni + 75 wt% SiO) demonstrated an ICE value of 84%. With the addition of Li in Ni doped SiO, the ICE value could be further increased to a nearly 100%.[78] By reacting SiO with Fe_2O_3 at 800 °C for 3 h in Ar, Yamamura and Iba prepared a Fe_2SiO_4 uniformly coated SiO anode, which exhibited a high ICE value of 89.3%.[113]

3. SiO_2-based anode materials

Silicon dioxide (SiO_2), also known as silica, is one of the most abundant materials on the earth. Both amorphous and various crystalline polymorphs of SiO_2 have been commonly found in nature. For example, quartz, a crystalline polymorph of SiO_2, is the major constituent of sand, while amorphous SiO_2 has been widely found in various living organisms, such as diatoms, rice husks, and reed leaves.[114–122]

3.1 Lithiation behavior of SiO_2

In early studies, SiO_2 was believed to be electrochemically inactive towards Li.[123] Actually, it was regarded as an inert matrix, buffering the volume expansion of active components upon lithiation. In 2001, Zhou *et al.* found that commercially available SiO_2 nanoparticles (~7 nm) could react with Li, providing a specific capacity of ~400 mA h g^{-1} (Table 2).[124]

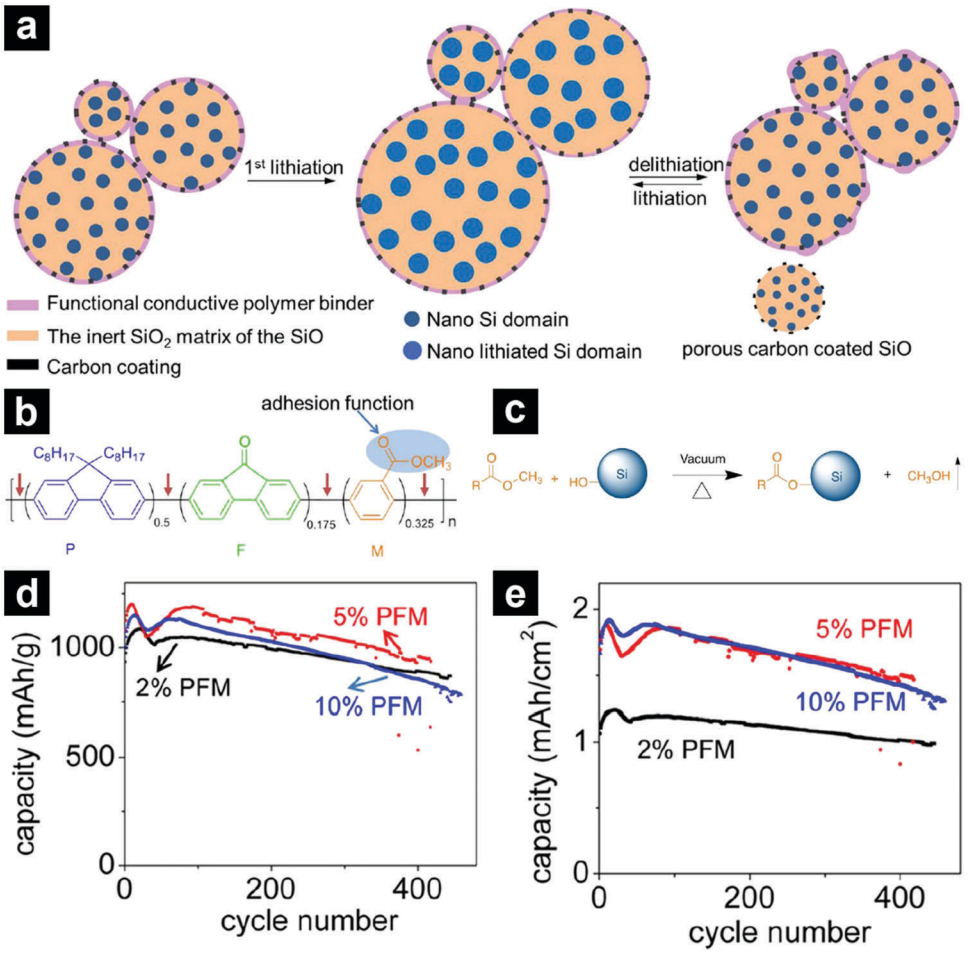

Fig. 8 Schematic illustration of a SiO-based electrode with low-concentration functional conductive polymer binder and high-concentration SiO/C (a). Chemical structure of the PFM functional conductive polymer binder with both strong adhesion and electrical conduction functionalities (b). Trans-esterification reaction between the ester functional group of the PFM binder and the surface Si–OH group, providing strong adhesion (c). Cycling performances of SiO anodes with 2, 5, 10 wt% PFM binder at 200 mA g^{-1} (d and e). Reproduced with permission from ref. 84. Copyright 2014, American Chemical Society.

In 2008, Wang and co-workers provided direct experimental evidence on the electrochemical reduction of SiO_2 through solid-state nuclear magnetic resonance (NMR), X-ray photoelectron spectroscopy (XPS), high-resolution transmission electron microscopy (HRTEM), and selected area electron diffraction (SAED).[125] They prepared a nano-SiO_2/hard carbon composite by a hydrothermal reaction and high-temperature carbonization; the resultant composite demonstrated a reversible capacity of 630 mA h g^{-1}. Using XPS, HRTEM, and SAED, Fu *et al.* also demonstrated the electrochemical activity of SiO_2 towards Li.[126] They prepared a SiO_2 thin-film electrode by reactive radio frequency sputtering, and the thin-film electrode exhibited discharge capacities of 416–500 mA h g^{-1} for 100 cycles.

To date, the reaction mechanism between Li and SiO_2 has not been well understood; there is still debate on the reaction pathway and final products. Theoretical computations and *in situ* TEM were used to reveal the lithiation of SiO_2.[127–130] Using density functional theory (DFT) and molecular dynamics (MD) simulations, Zhao *et al.* concluded that neither interstitial Li, nor the formation of Li_2O and Si–Si bonds (full reduction) were energetically favorable. Instead, the lithiation could proceed through partial reduction, namely, two Li attacked and broke a Si–O bond.[127] Through first-principles calculations, Balbuena *et al.* revealed that Li was incorporated *via* breaking Si–O bonds and partial reduction of the Si atoms.[129] The breaking of Si–O bonds became less favorable at high lithiation degrees and was accompanied by Si–Si bond formation and nucleation of Li_6O complexes. Leivia's group calculated the free energy of reaction for the lithiation of SiO_2 for different products using DFT. They found the formation of $Li_2Si_2O_5$ is energetically most favorable.[131] In another study, they extended the analysis to the free energy of reactions involving the lithiation of SiO_2 as a function of cell potential. It was found that the most probable lithiation product was cell-potential-dependent.[132]

Zhao *et al.* integrated a single SiC@SiO_2 core@shell nanowire into a nanobattery setup (Fig. 10a) and monitored the structural evolution of the nanowire during *in situ* electrochemical lithiation/de-lithiation by TEM and SAED.[128] The pristine SiC@SiO_2 nanowire consisted of a crystalline SiC core and a uniform amorphous SiO_2 shell with a thickness of 5–10 nm. The SiC core was inactive towards Li and did not change upon lithiation. While for the SiO_2 shell, its thickness increased and

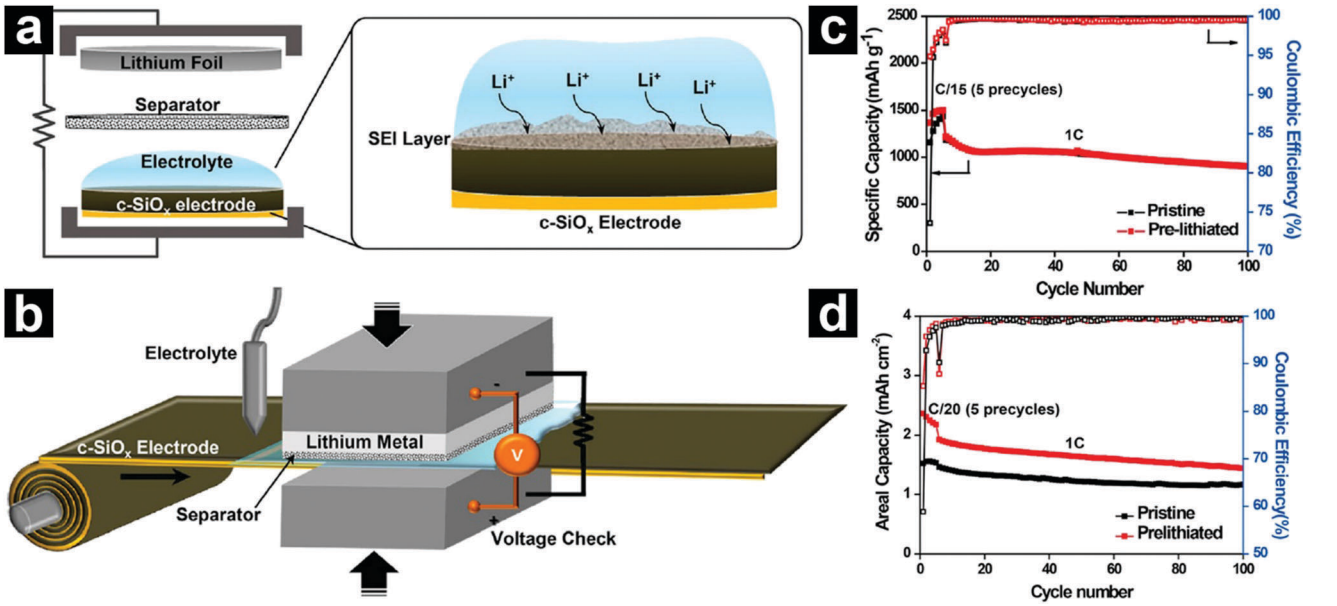

Fig. 9 Schematic illustration of the pre-lithiation process (a) and a scalable roll-to-roll pre-lithiation process (b). Cycling performances of pristine and pre-lithiated SiO in half-cells (c). 1C = 1500 mA g^{-1}. Cycling performances of pristine and pre-lithiated SiO in SiO/NCA full cells (d). Reproduced with permission from ref. 112. Copyright 2016, American Chemical Society.

Table 2 Electrochemical performances of SiO_2-based anode materials

Year	Sample	Initial discharge/charge capacity (mA h g^{-1})	ICE (%)	Cycling performance	Ref.
2001	SiO_2	~940/~415	~44	—	124
2008	SiO_2/C	~630/~1010	~62	—	125
2008	SiO_2	539/388	72	~500 (100 cycles)	126
2011	SiO_2/C	891/536	60	~500 (55 cycles)	148
2011	SiO_2	980/323	33	334 (500 cycles)	143
2011	PMO	970/276	28	242 (300 cycles)	144
2012	SiO_2	2243/827	37	~660 (200 cycles)	139
2013	SiO_2	3084/1457	47	919 (30 cycles)	146
2013	SiO_2/C	835/505	60.5	600 (100 cycles)	171
2014	SiO_2	2404/1040	43.3	1247 (100 cycles)	147
2014	SiO_2	1134.5/622.1	54.8	876.7 (500 cycles)	137
2014	SiO_2/C	1380/841	61	780 (350 cycles)	152
2014	SiO_2/C	712/418	59	560 (30 cycles)	149
2015	SiO_2/C	~2900/~1200	42	800 (100 cycles)	150
2015	SiO_2/C	—	—	636 (200 cycles)	153
2015	SiO_2/C	2547/1438	56.5	1055 (150 cycles)	155
2015	SiO_2/C	1071/629	58.7	658 (100 cycles)	163
2015	SiO_2/C	1050/697	66.4	620 (300 cycles)	173
2017	SiO_2/C	880/530	68	441 (500 cycles)	157
2017	SiO_2/Ni	1195/676	56.5	672 (50 cycles)	174

its surface roughened during lithiation, forming a wavy structure after the first lithiation (Fig. 10b). Through SAED characterization, it was found that crystalline Li_2O was formed at the early stage of lithiation, and further lithiation led to the formation of a mixture of Li_4SiO_4 and Li_2O, the so-called Li–Si–O glass (Fig. 10c). Theoretical studies revealed that the electrical conductivity of SiO_2 was significantly enhanced during lithiation/de-lithiation, while the Li^+ diffusivity decreased.

3.2 Electrochemical performance of SiO_2

3.2.1 Bare SiO_2 anode materials. Despite its high theoretical capacity (1965 mA h g^{-1}), bulk SiO_2 shows little electrochemical activity towards Li due to the sluggish Li^+ diffusivity and poor intrinsic electrical conductivity. Reducing the particle size has been demonstrated to be an effective strategy to shorten the Li^+ diffusion length and enhance the electrochemical activity of certain electrode materials.[133–136] Therefore, efforts have been dedicated to preparing fine-sized SiO_2. For example, Jiao *et al.* synthesized Stöber SiO_2 spheres with an average size of ~400 nm through a sol–gel process, which delivered a first charge capacity of 622 mA h g^{-1} with an ICE value of 54.8%.[137] After 500 discharge/charge cycles, the charge capacity increased to 877 mA h g^{-1}. Mechanical milling is an effective strategy to reduce the particle size of SiO_2. Zheng and co-workers synthesized

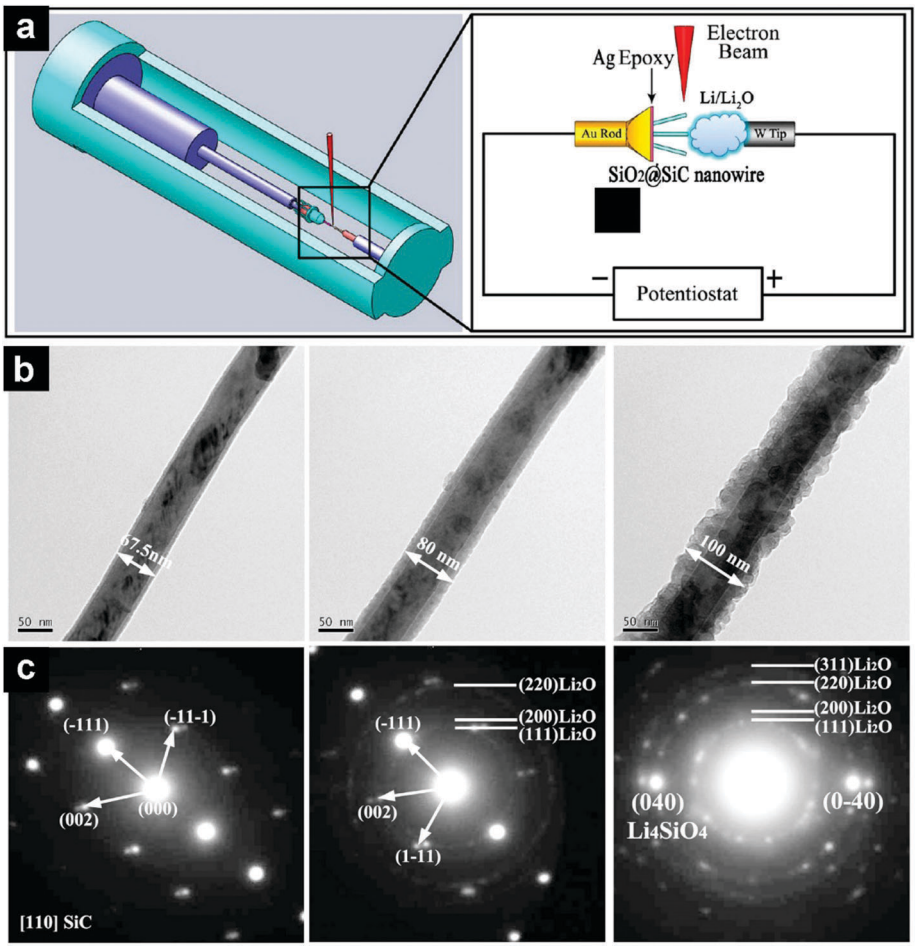

Fig. 10 Schematic illustration of a nanobattery consisting of a SiC@SiO_2 single-nanowire working electrode and Li/Li_2O counter electrode/electrolyte (a). TEM images of a SiC@SiO_2 nanowire from the pristine state to the end of first lithiation (b). The corresponding SAED patterns at given lithiation states (c). Reproduced with permission from ref. 128. Copyright 2014, American Chemical Society.

submicron SiO_2 by planetary ball milling bulk SiO_2, and the optimized sample provided a specific capacity of $\sim$600 mA h g^{-1} for 150 cycles.[138] By HEMM quartz, a common crystalline polymorph of SiO_2, a sample (HEMM-treated SiO_2) consisting of nanosized Si embedded in amorphous SiO_2 was obtained.[139] The HEMM-treated SiO_2 exhibited an initial charge capacity of 827 mA h g^{-1}, retaining 80% of the capacity after 200 cycles. Hollow structures with hollow cavities for volume variation accommodation and thin shells for Li^+ diffusion represent a promising family of electrode architecture.[140–142] Various hollow structured SiO_2, such as hollow spheres,[143–145] hollow cubes,[146] hollow nanobelts, and nanotubes,[147] have been explored in lithium storage. Nakashima reported the synthesis of SiO_2 hollow nanospheres (Fig. 11a and b) with a uniform size of $\sim$30 nm using poly(styrene-*b*-2-vinyl pyridine-*b*-ethylene oxide) (PS-PVP-PEO) triblock copolymer as the structure directing agent.[143] The resultant SiO_2 hollow nanospheres delivered a capacity of 242 mA h g^{-1} after 300 cycles.[144] Chen's group constructed hollow SiO_2 nanocubes (Fig. 11c and d) through a hard-templating method.[146] The nanospheres demonstrated a stable discharge capacity of 334 mA h g^{-1} after 500 cycles. Using a similar approach, the same group also prepared periodic organosilica (PMO) hollow SiO_2 nanocubes which exhibited a first discharge capacity of 3084 mA h g^{-1} and an ICE of 47%. The capacity decreased quickly to 919 mA h g^{-1} after 30 cycles. Ozkan *et al.* fabricated SiO_2 nanotubes (Fig. 11e and f) using commercial anodic aluminum oxide (AAO) as the hard template and polydimethylsiloxane as the precursor.[145] When applied as the anode in LIBs, the SiO_2 nanotubes displayed first discharge and charge capacities of 2404 and 1040 mA h g^{-1}, respectively. Besides high specific capacity, the SiO_2 nanotubes also demonstrated impressive rate capability and cyclic performance.

3.2.2 SiO_2/C hybrid anode materials. Among the silicon oxide-based materials, SiO_2 possesses the lowest conductivity. Many efforts have been dedicated to improving the conductivity of SiO_2 through compositing with carbon.[125,148] Besides enhancing the electrical conductivity, coupling with carbon can also buffer the volume fluctuation of SiO_2. Thus, the SiO_2/C composites usually manifested superior cyclability.

Among the various SiO_2/C composites, porous, especially mesoporous SiO_2/C hybrids have attracted much attention.[149–156] The porous structure not only provides free space for the volume expansion of SiO_2 upon lithiation but also enables rapid Li^+ diffusion. As a result, both the cycling stability and rate capability

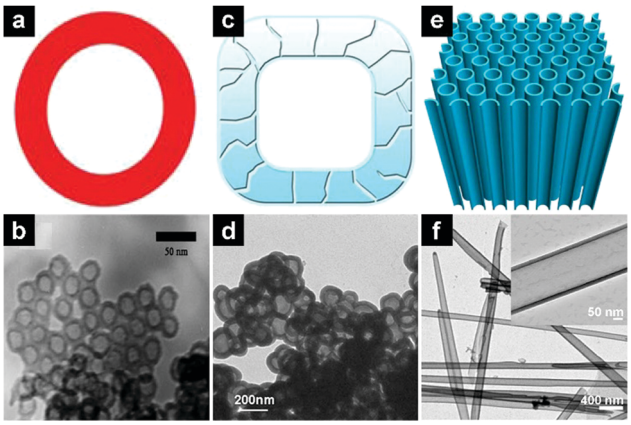

Fig. 11 Schematic illustrations and TEM images of SiO_2 hollow nanospheres (a and b), hollow porous SiO_2 nanocubes (c and d), and SiO_2 nanotubes (e and f). (a and b) Reproduced with permission from ref. 143. Copyright 2011, Royal Society of Chemistry. (c and d) Reproduced with permission ref. 146. Copyright 2013, Nature Publishing Group. (e and f) Reproduced with permission from 147. Copyright 2014, Nature Publishing Group.

can be enhanced. For example, Wu and co-workers fabricated a porous bicontinuous SiO_2/C nanocomposite using tetraethoxysilane (TEOS) as the SiO_2 precursor and sucrose as the carbon source.[149] In the constructed composite, the continuous SiO_2 framework provided abundant active sites for lithium storage; the carbon not only wired the whole composite, but also enhanced the structural integrity; the nanopores effectively accommodated the volume expansion of SiO_2 and enabled the rapid diffusion of Li^+. The porous SiO_2/C composite manifested a capacity of 560 mA h g^{-1} after 30 cycles. Through a multi-constituent co-assembly approach, the same group fabricated a N-doped ordered mesoporous carbon/SiO_2 nanocomposite with unique interpenetrating SiO_2 and carbon frameworks (Fig. 12a and b).[150] The mesoporous SiO_2/C composite delivered a capacity of ~800 mA h g^{-1} after 100 cycles. Using a similar approach, Wang and co-workers prepared a mesoporous SiO_2/C composite with a reversible capacity of 670 mA h g^{-1}.[151]

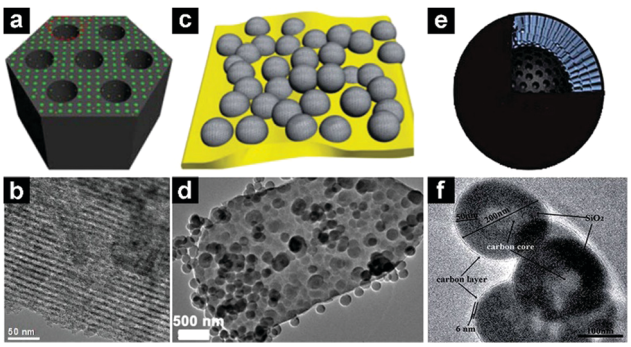

Fig. 12 Schematic illustrations and TEM images of a mesoporous SiO_2/C composite (a and b), plum-pudding like mesoporous SiO_2 nanosphere/flake graphite (c and d), and carbon core/mesoporous SiO_2/carbon shell three-layer structure (e and f). (a and b) Reproduced with permission from ref. 150. Copyright 2015, Royal Society of Chemistry. (c and d) Reproduced with permission from ref. 154. Copyright 2015, Royal Society of Chemistry. (e and f) Reproduced with permission from ref. 155. Copyright 2015, Royal Society of Chemistry.

By coating ordered mesoporous SiO_2 with carbon, Zhao *et al.* designed a SiO_2/C composite anode, which demonstrated a high specific capacity of 780 mA h g^{-1} after 350 cycles.[152] Through a hydrothermal method, Zhang and co-workers fabricated a plum-pudding like mesoporous SiO_2 nanosphere/flake graphite composite (Fig. 12c and d).[154] The obtained SiO_2/FG composite exhibited a high capacity of 702 mA h g^{-1} after 100 cycles. A carbon core@mesoporous silica@carbon shell three-layer structure (Fig. 12e and f) was designed by Cao *et al.*[155] The product delivered a capacity of 1055 mA h g^{-1} after 150 cycles.

To integrate the advantages of both hollow structures and carbon coating, hollow structured SiO_2/C composites have also been explored.[157–161] Zhang and co-workers prepared SiO_2/C mesoporous hollow spheres by combining a sol–gel process and carbon coating.[157] The SiO_2/C mesoporous hollow spheres demonstrated a capacity of 441 mA h g^{-1} after 500 cycles at 500 mA g^{-1}. At a lower current density of 100 mA g^{-1}, the specific capacity could reach 695 mA h g^{-1}. Combining an aerosol spray drying process with polyacrylonitrile (PAN) coating and carbonization, Wang and co-workers prepared a hollow core–shell structured SiO_2/C composite, which possessed a high specific capacity of 670 mA h g^{-1} after 100 cycles.[161]

Besides porous/hollow structures, various other nanostructured SiO_2/C composites have also been extensively studied in lithium storage.[162–171] These nanostructures include SiO_2/C nanofibers,[162,163,172] SiO_2/C spheres,[173] SiO_2/graphene,[165] and SiO_2/C/graphene spheres.[166]

3.2.3 SiO_2/metal hybrid anode materials. Coupling SiO_2 with conductive metal has also been demonstrated to be effective in electrical conductivity improvement and electrochemical activity enhancement.[174–176] For example, Zhou, Mai, and co-workers constructed a novel SiO_2/Ni nanocomposite with hierarchical hollow spherical structure (Fig. 13a–c) through the reduction of nickel silicate in H_2/Ar (5%/95%).[174] The obtained SiO_2/Ni nanocomposite has the following structural merits for lithium storage: (I) hollow spherical structure for volume fluctuation accommodation and strain relaxation; (II) ultrathin nanosheet building blocks for efficient Li^+ diffusion; and (III) ultrafine Ni nanoparticle decoration for electron transfer enhancement. Benefited from these unique structural features, the SiO_2/Ni hierarchical hollow spheres demonstrated high specific capacities of 672 mA h g^{-1} after 50 cycles at 100 mA g^{-1} and 337 mA h g^{-1} after 1000 cycles at 10 A g^{-1} (Fig. 13d and e). It is anticipated that this approach could be generalized for the preparation of other SiO_2/metal nanocomposites.

4. SiO_x-based anode materials

Just like SiO and SiO_2, nonstoichiometric silicon suboxides (SiO_x) have also been identified as an attractive high-capacity anode material for next-generation LIBs, especially when the O content is lower than 1.0 (Si-rich SiO_x).[177]

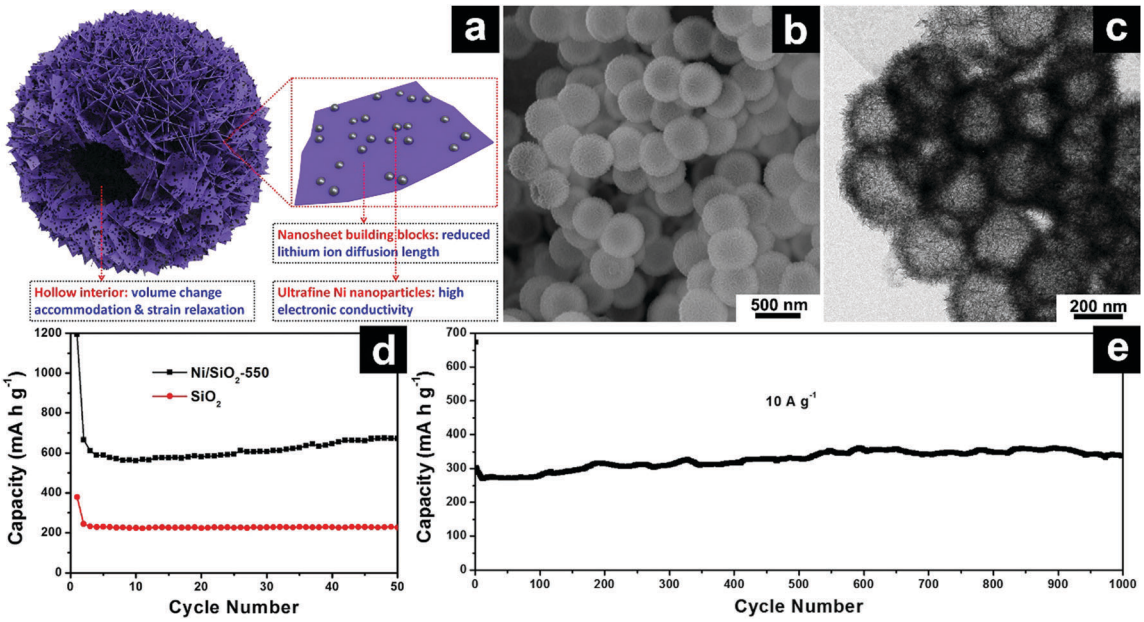

Fig. 13 Schematic illustration of SiO_2/Ni hierarchical hollow microspheres constructed by ultrafine Ni nanoparticle decorated SiO_2 nanosheets (a); SEM (b) and TEM (c) images of SiO_2/Ni hierarchical hollow spheres; cycling performances of SiO_2/Ni hierarchical hollow spheres at 100 mA g^{-1} (d) and 10 A g^{-1} (e). Reproduced with permission from ref. 174. Copyright 2017, Wiley-VCH.

4.1 Lithiation behavior of SiO_x

The lithiation behavior of $SiO_{1/3}$ was investigated by Chou and Hwang by DFT calculations.[177] It was found that the $SiO_{1/3}$ host matrix gradually disintegrated into smaller fragments with lithiation. Meanwhile, the Si–O–Si units ruptured and the O atoms tended to be surrounded by Li atoms (Fig. 14). With increasing Li contents, the Si–Li coordination number increased monotonically to around 10 in amorphous $Li_4SiO_{1/3}$, whereas the O–Li coordination number tended to saturate far before full lithiation at around 6.

4.2 Electrochemical performances of SiO_x

4.2.1 Bare SiO_x anode materials. The research on bare SiO_x-based anodes has mainly focused on studying the effect of O contents in SiO_x on their electrochemical performances.[178–185]

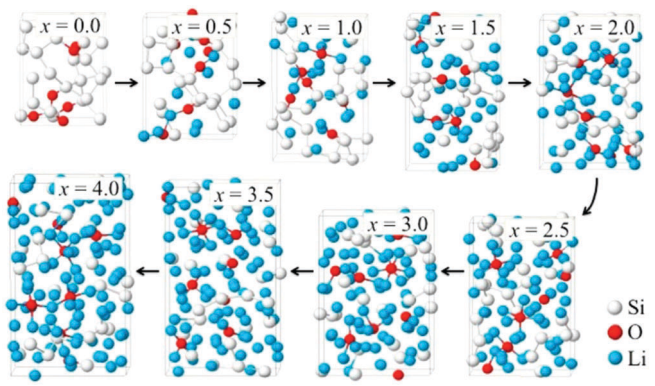

Fig. 14 Structural evolution of amorphous $Li_xSiO_{1/3}$ with increasing Li contents. Reproduced with permission from ref. 177. Copyright 2013, American Chemical Society.

Early in 2002, Yang *et al.* performed a comparative study on $SiO_{0.8}$, SiO, and $SiO_{1.1}$.[57] It was found that the decrease in O content in SiO_x enhanced the reversible capacity as well as the ICE,[186] but sacrificed the cycling stability. This conclusion was further confirmed by several groups independently.[181–185]

It is generally accepted that the Si-rich SiO_x possesses high capacity but suffers from poor cycling performance, while the O-rich SiO_x is beneficial for volume change accommodation. To integrate the advantages of both components, Yan and co-workers designed a SiO_x/SiO_y bi-layer nano-membrane anode (Fig. 15a).[187] The inner Si-rich SiO_y layer (y = 0.5) contributed a high Li storage capacity to the composite; meanwhile, the outer O-rich SiO_x layer (x = 1.85) acted as a buffering layer for volume change accommodation. Due to the smart design, the SiO_x/SiO_y bi-layer nano-membrane delivered a specific capacity of ~1300 mA h g^{-1} after 100 cycles.

4.2.2 SiO_x/C hybrid anode materials. Compared to unmodified SiO_x, the SiO_x/C composites demonstrated better cyclability and rate capability due to the excellent electrical conductivity and volume change accommodation ability of carbon. The sol–gel process of silane has been demonstrated to be an effective approach for the construction of SiO_x/C composite anode materials. For example, a series of SiO_x/C composites, such as SiO_x/C spheres,[188] SiO_x/graphene/carbon[189] SiO_x/C nanorods,[190] and SiO_x/multi-walled carbon nanotube/carbon (SiO_x/MWCNT/C), have been fabricated by Li *et al.* through the hydrolysis and condensation of ethyltriethoxysilane ($CH_3CH_2Si(OCH_2CH_3)_3$). All these materials demonstrated high specific capacities (600–800 mA h g^{-1}) and excellent cycling performances (150–450 cycles). Using the sol–gel process of TEOS, Zhao *et al.* synthesized a series of SiO_x/C composite anode materials, including core@shell nanoparticles (Table 3),[191,192] mesostructured architectures,[152] and dual-phase glass.[193] These materials delivered

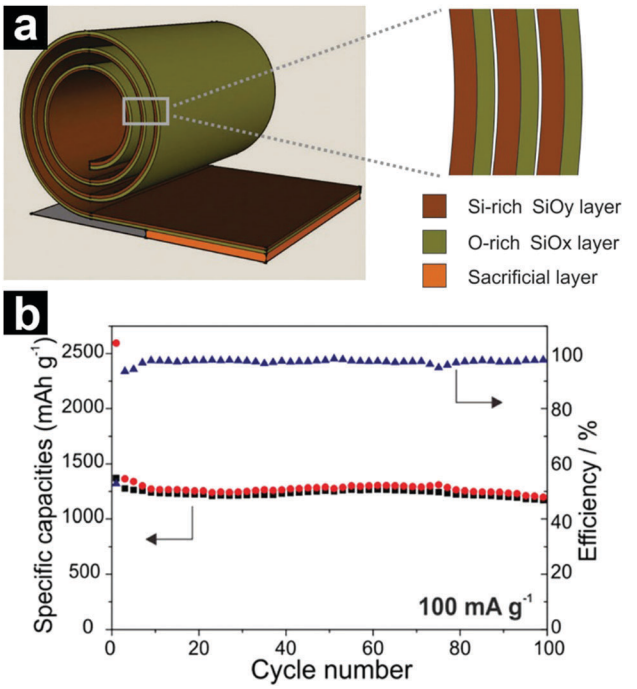

Fig. 15 Schematic structure of the rolled-up SiO_x/SiO_y bi-layer nanomembrane (a); cycling performance of the SiO_x/SiO_y bi-layer nanomembrane at a current density of 100 mA g^{-1} (b). Reproduced with permission from ref. 187. Copyright 2014, Wiley-VCH.

high reversible capacities of 600–1000 mA h g^{-1} with stable cycling (50–350 cycles). Using the sol–gel reaction of triethoxysilane, Kim *et al.* prepared hydrogen silsesquioxane ($HSiO_{1.5}$) nanospheres.[194] After high-temperature annealing and carbon coating, $Si/SiO_x/C$ nanospheres could be obtained. The resultant $Si/SiO_x/C$ nanospheres manifested a reversible capacity of ~950 mA h g^{-1} at 200 mA g^{-1}, retaining 740 mA h g^{-1} after 100 cycles. Wang *et al.* designed a $SiO_x/C/rGO$ ternary nanocomposite using TEOS as the silicon precursor.[195] The $SiO_x/C/rGO$ ternary nanocomposite exhibited a very high capacity of 1284 mA h g^{-1} after 100 cycles. Recently, Zhou, Mai, and co-workers fabricated monodisperse and homogeneous SiO_x/C (Fig. 16a–c) composite microspheres through co-condensation of vinyltriethoxysilane and resorcinol/formaldehyde.[195] With the uniform dispersion of sub-nanosized SiO_x in amorphous carbon (Fig. 16d), high electrical conductivity and outstanding cycling stability could be achieved. When used as the anode materials for LIBs, the SiO_x/C composite microspheres demonstrated a high specific capacity of 689 mA h g^{-1} at 500 mA g^{-1} and a capacity retention of 91.0% after 400 cycles. Mai's group also prepared unique yolk@shell structured SiO_x/C composite microspheres through sol–gel synthesis, selective etching, and carbonization. To further improve the structural stability and electrical conductivity, they adopted a CVD process to coat the SiO_x/C with semi-graphitic carbon on both the exterior and interior surfaces (SiO_x/C-CVD) (Fig. 17a and b). The as-prepared SiO_x/C-CVD demonstrated a high reversible capacity (1165 mA h g^{-1} at 100 mA g^{-1}) as well as outstanding durability (972 mA h g^{-1} after 500 cycles at 500 mA g^{-1}) (Fig. 17c and d). The excellent electrochemical performance can be ascribed to the following two aspects: (I) the yolk@shell structure provides enough space for volume change accommodation. (II) The semi-graphitic carbon coating layers on the exterior and interior surfaces promote the electrical conductivity and structural integrity of the whole composite.[197]

Guo *et al.* prepared graphite-like SiO_x/C composites with SiO_x particles anchored in the carbon matrix uniformly (Fig. 18a).[198] Such a unique structure effectively addressed the disadvantages of SiO_x such as low mass loading, large volume change, and poor electrical conductivity. The resultant SiO_x/C demonstrated high reversible capacity (645 mA h g^{-1}), excellent cycling stability (≈90% capacity retention for 500 cycles), and impressive rate performance (Fig. 18b and c).

Guo's group also prepared flake-graphite-like SiO_x@G with SiO_x encapsulated in a graphene bubble film through a facile protonated chitosan assisted self-assembly process (Fig. 19a–c).[199] The unique structure enabled efficient electrical contact of SiO_x with amorphous carbon, and a high tap density with low

Table 3 Electrochemical performances of SiO_x-based anode materials

Year	Sample	Initial discharge/charge capacity (mA h g^{-1})	ICE (%)	Cycling performance	Ref.
2011	SiO_x/C	2224/1052	47.3	~800 (50 cycles)	191
2013	$NiSi_x@SiO_x$	4058/1737	42.8	~800 (100 cycles)	201
2014	SiO_x/C	1380/841	61	780 (350 cycles)	185
2014	SiO_x/SiO_y	2595/1372	53	~1300 (100 cycles)	187
2014	$Si/SiO_x/C$	1629/951	58.4	740 (100 cycles)	194
2014	$SiO_x/C/rGO$	2403/1226	51	1284 (100 cycles)	195
2015	SiO_x/graphene/C	896/607	67.7	630 (250 cycles)	189
2015	SiO_x/C	1160/820	70.7	630 (150 cycles)	188
2015	SiO_x/C	~1150/644	56	840 (100 cycles)	193
2015	SiO_x/C	1475/1015	68.8	817 (100 cycles)	192
2016	SiO_x/C	3097/1394	45	1230 (200 cycles)	119
2016	SiO_x/C	1324/906	68.4	720 (350 cycles)	190
2016	SiO_x/MWCNT/C	1093/720	66	621 (450 cycles)	203
2016	SiO_x/C	999/466	46.6	582 (100 cycles)	120
2017	$FeSi@Si/SiO_x$	1550/803	51.8	727 (600 cycles)	202
2018	SiO_x/C	1460/999	66.1	853 (150 cycles)	196
2018	SiO_x/C	1734/1165	67.4	972 (500 cycles)	197
2018	SiO_x/C	785/645	82.2	580 (500 cycles)	198
2018	SiO_x@GO	1510/1042	69	740 (1000 cycles)	199

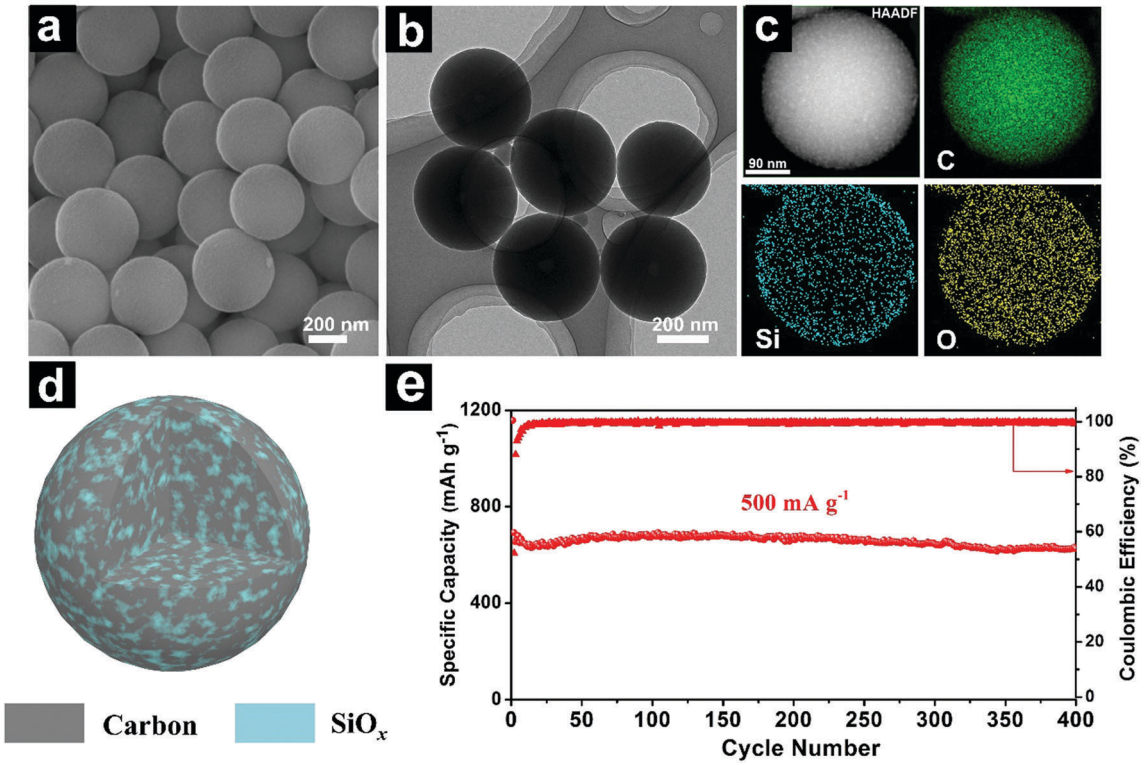

Fig. 16 SEM (a), TEM (b) and EDS elemental mapping (c) images of SiO_x/C composite microspheres; schematic illustration (d) of the homogeneous SiO_x/C composite microspheres with; cycling performances of SiO_x/C composite microspheres at 500 mA g^{-1} (e). Reproduced with permission from ref. 196. Copyright 2018, Elsevier Ltd.

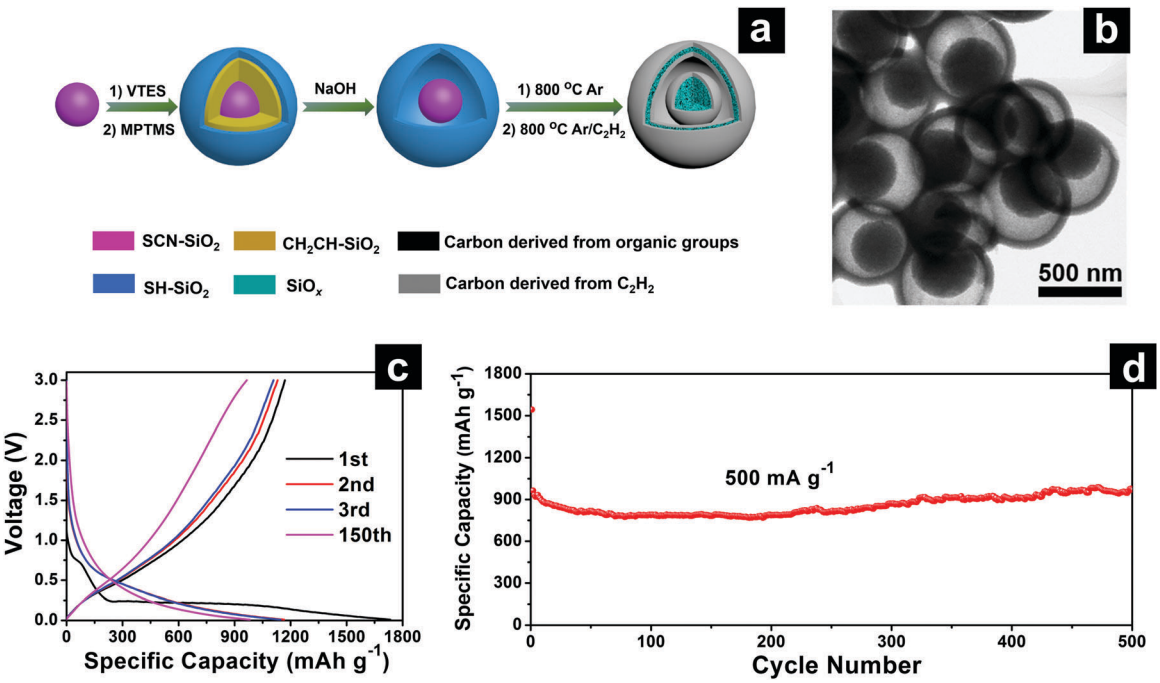

Fig. 17 Schematic illustration of yolk@shell SiO_x/C microspheres with semi-graphitic carbon coating on the exterior and interior surfaces (SiO_x/C-CVD) (a); TEM (b); discharge–charge profiles (c) of SiO_x/C-CVD; cycling performances (d) of SiO_x/C and SiO_x/C-CVD at 500 mA g^{-1}. Reproduced with permission from ref. 197. Copyright 2018, Elsevier Ltd.

particle agglomeration/exposure; mechanical strength can also be realized. The obtained SiO_x@G exhibited a capacity far above the theoretical capacity of graphite and the retention after 1000 cycles at 1 A g^{-1} is 80%.

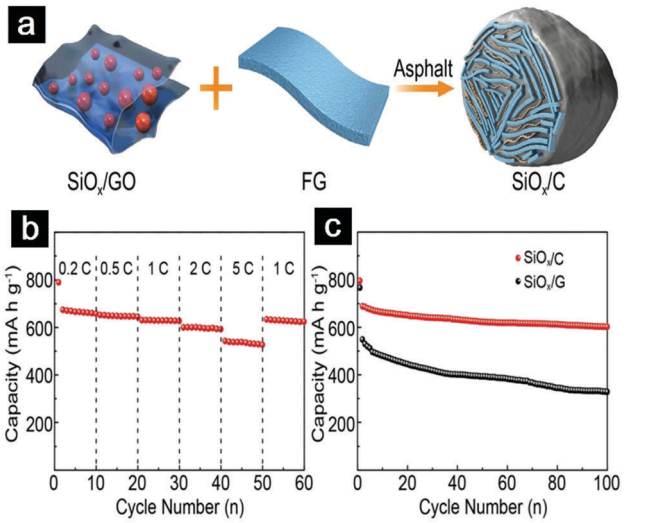

Fig. 18 Schematic illustration showing the synthetic process of SiO_x/C hydrogels (a); rate capabilities of SiO_x/C anodes at a mass loading of 3.5 mg cm^{-2} (b); cycling performance of SiO_x/G and SiO_x/C anodes at a pressing density of 1.3 g cm^{-3} (c). Reproduced with permission from ref. 198. Copyright 2018, Wiley-VCH.

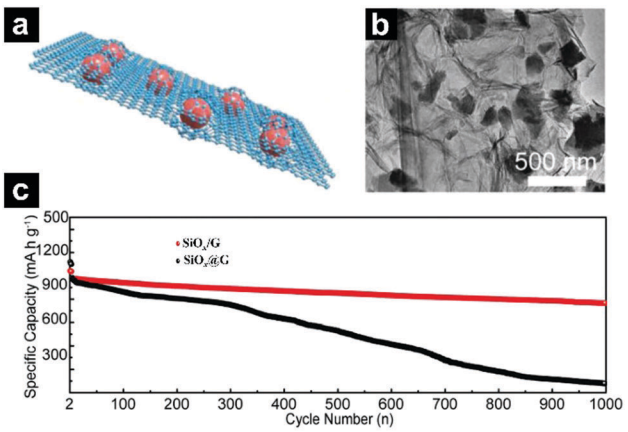

Fig. 19 Schematic illustration (a) and TEM images (b) of flake-graphite-like SiO_x@G; cycling performances of SiO_x/G and SiO_x@G under a current density of 200 mA g^{-1} for the first 3 cycles and 1000 mA g^{-1} for later cycles (c). Reproduced with permission from ref. 199. Copyright 2018, Wiley-VCH.

4.2.3 SiO_x/metal hybrid anode materials. Besides SiO_x/C composites, SiO_x/metal hybrids are also appealing for lithium storage.[200–202] For example, $NiSi_x$@SiO_x heterostructured nanowires (Fig. 20a and b) prepared by CVD exhibited a reversible capacity of 1737 mA h g^{-1} (based on the mass of SiO_x).[201] The capacity decreased slowly upon cycling, remaining at 800 mA h g^{-1} after 100 cycles. In another study, core@shell structured FeSi alloy@Si/SiO_x was prepared through controlled oxidation of FeSi alloy (containing 73.3 wt% Si and 21.4 wt% Fe) in air.[202] Impressively, the core@shell structured FeSi alloy@Si/SiO_x delivered capacities of 967 mA h g^{-1} after 50 cycles at 50 mA g^{-1} and 727 mA h g^{-1} after 600 cycles at 200 mA g^{-1}. At a current density of 1000 mA g^{-1}, 86% of the capacity (compared to the capacity at the third cycle) could be retained after 1000 cycles.

5. SiOC-based anode materials

Silicon oxycarbide (SiOC) refers to a family of carbon-containing silicate ceramics wherein O and C atoms share bonds with Si in the amorphous network.[204] In the 1990s, Dahn *et al.* first demonstrated the lithium storage capability of SiOC glass (Table 4).[205–209] Since then, significant efforts have been dedicated to the preparation of SiOC-based anode materials.[210,211]

5.1 Microstructure and lithium storage mechanism of SiOC

5.1.1 Microstructure of SiOC. It is necessary to mention the microstructure of SiOC before discussing its lithium storage mechanism and performance. SiOC is a high-temperature ceramic with an open polymer-like network structure consisting of an amorphous SiOC glass phase and a free carbon phase.[202,213] Its detailed microstructure can be represented by the nanodomain model.[214] In such a model, the free carbon forms a continuous matrix, encapsulating the SiOC nanodomains. SiO_4 tetrahedra locate at the center of the SiOC nanodomains and SiO_nC_{4-n} $(0 \leq n < 4)$ tetrahedra sit at the interface of SiOC glass and free carbon phases.

5.1.2 Lithium storage mechanism of SiOC. The lithium storage mechanism of SiOC is an interesting topic. However, the origin of lithium storage activity of SiOC is still a controversial issue.[212,215–220] Kanamura *et al.* observed three types of electrochemically active sites by employing 7Li NMR: interstitial spaces or edges of the graphene layers, the amorphous SiOC glass phase, and the micropores.[215] Among the three types of active sites, the interstitial spaces or edges of the graphene layers were believed to be the major active site for lithium storage. Using ^{29}Si NMR and XPS, however, Liu *et al.* found that the major share of the reversible capacity of SiOC was obtained from the alloy reaction between Li and the SiOC glass phase.[212,217] Among the different $SiOnC_{4-n}$ units, the SiO_2C_2, SiO_3C, and SiO_4 units were electrochemically active and contributed to the reversible capacity; however, the $SiOC_3$ units only contributed to the irreversible capacity and were transformed into SiC_4 units without electrochemical activity. Using first-principles calculations, Liao, Zheng, and co-workers investigated the lithiation behavior of SiOC with different carbon contents.[218] It was found that the Li atoms preferred to bond with O atoms and stayed in the voids near the carbon atoms.

5.2 Electrochemical performance optimization of SiOC

5.2.1 Bare SiOC anode materials. Although the polymer-derived ceramic SiOC contains a free carbon phase, we consider it as pristine SiOC herein unless otherwise mentioned.

Pristine SiOC are commonly synthesized *via* the pyrolysis of Si-containing polymer precursors, such as polysiloxane and polysilsesquioxane.[205,208,221–226] For example, Dahn's group reported the synthesis of SiOC anodes from polymethylphenylsiloxane (PMPS) and polyphenylsesquisiloxane (PPSS).[205] Lee *et al.* reported the simple and scalable production of SiOC from a commercial phenyl-rich silicone oil precursor.[225] Impressively, the obtained SiOC demonstrated a stable specific capacity of ~800 mA h g^{-1} for up to 250 cycles. To tailor the chemical

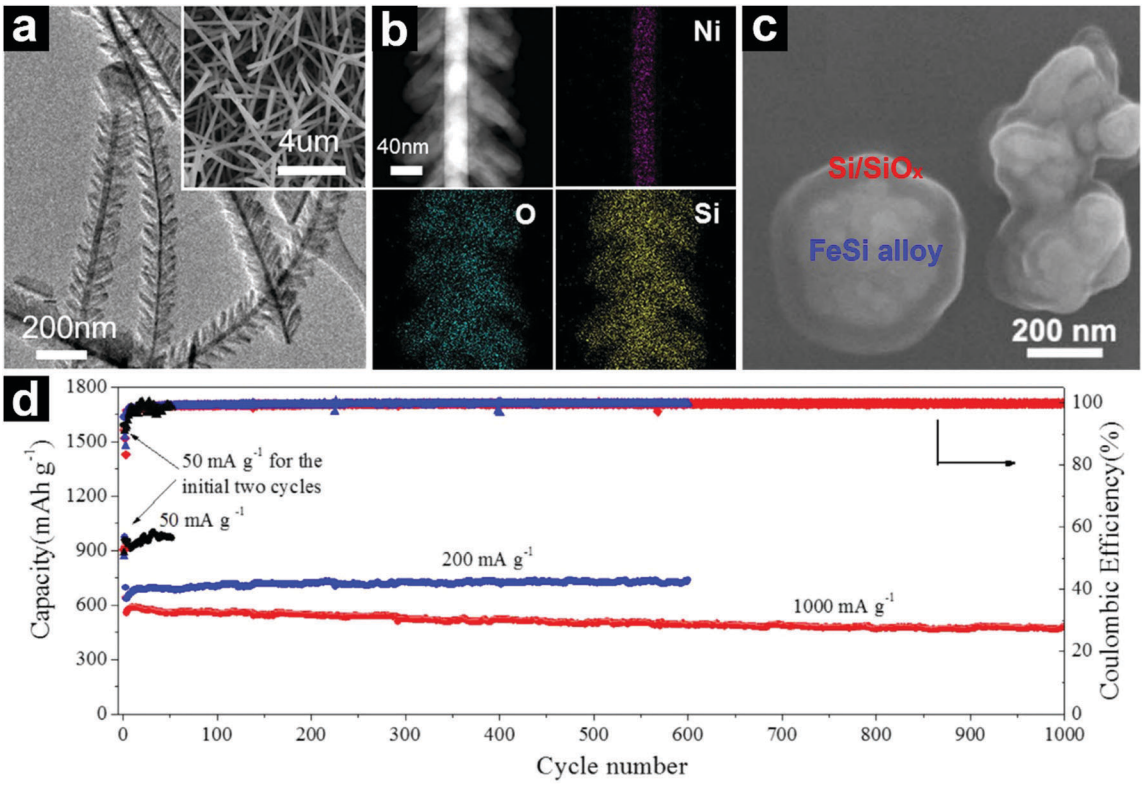

Fig. 20 TEM and SEM (inset) images of $NiSi_x$@SiO_x heterostructured nanowires (a); STEM HAADF image and EDX elemental mappings of an individual $NiSi_x$@SiO_x heterostructured nanowire (b); SEM image of core@shell structured FeSi alloy@Si/SiO_x (c); cycling performances of the core@shell structured $FeSi_x$@Si/SiO_x at current densities of 50–1000 mA g^{-1} (d). (a and b) Reproduced with permission from ref. 201. Copyright 2013, Elsevier Ltd. (c and d) Reproduced with permission from ref. 202. Copyright 2017, Elsevier Ltd.

Table 4 Electrochemical performances of SiOC-based anode materials

Year	Sample	Initial discharge/charge capacity (mA h g^{-1})	ICE (%)	Cycling performance (mA h g^{-1})	Ref.
1994	SiOC	~900/~550	61–67	~400 (25)	205
2011	SiOC thin film	~1500/~1100	73	~1000 (45)	211
2012	SiOC thin film (based on the mass of Si)	1403/4731	30	842 (7200)	230
2014	SiOC/Sn	1022/651	64	562 (110)	243
2016	SiOC/rGO	~1030/~700	~68	588 (1020)	213
2016	SiOC	~1200/676	~56	804 (250)	225

composition and microstructure of SiOC, extra organic species, such as pitch, citric acid, and acenaphthylene, can also be introduced during the synthesis.[206,209,227,228]

Besides SiOC powdered samples, SiOC-based thin films have also been constructed for LIB applications.[211,229–234] Raj *et al.* prepared SiOC thin films by spraying a Si-containing polymer precursor on Cu with subsequent annealing.[211] The SiOC thin-film anode with a thickness of 0.5 μm demonstrated a reversible capacity of ~1100 mA h g^{-1} and an ICE value of 73%. Osaka's group developed an electrodeposition method for the fabrication of SiOC-based thin films using $SiCl_4$ as the precursor, $LiClO_4$ in propylene carbonate /ethylene carbonate as the electrolyte.[229–234] It is believed that the electrodeposition of Si is accompanied by the decomposition of the organic solvent, resulting in the formation of SiOC-based films.[232] Based on the mass of Si, the specific capacity of the as-synthesized SiOC thin films reached 1045 mA h g^{-1} at the 2000th cycle and 842 mA h g^{-1} at the 7200th cycle.[230]

5.2.2 SiOC/C hybrid anode materials. Despite its high specific capacity, the lithium storage performances of pristine SiOC are still far from practical applications. Thus, efforts have been devoted to constructing SiOC/C hybrids for further enhancement of electrochemical performance.[213,235–242] More than a decade ago, exfoliated graphite was used to couple with SiOC for electrical conductivity improvement.[235,236]

Recently, CNTs,[237,238] carbon nanofibers,[239] graphene,[213,240] and carbon paper[241] were also employed for electrochemical performance enhancement. Interestingly, when these one-dimensional/two-dimensional carbon materials were introduced, free-standing SiOC-based electrodes could be obtained. As an excellent example, Singh *et al.* constructed a novel free-standing SiOC/rGO composite paper electrode through vacuum

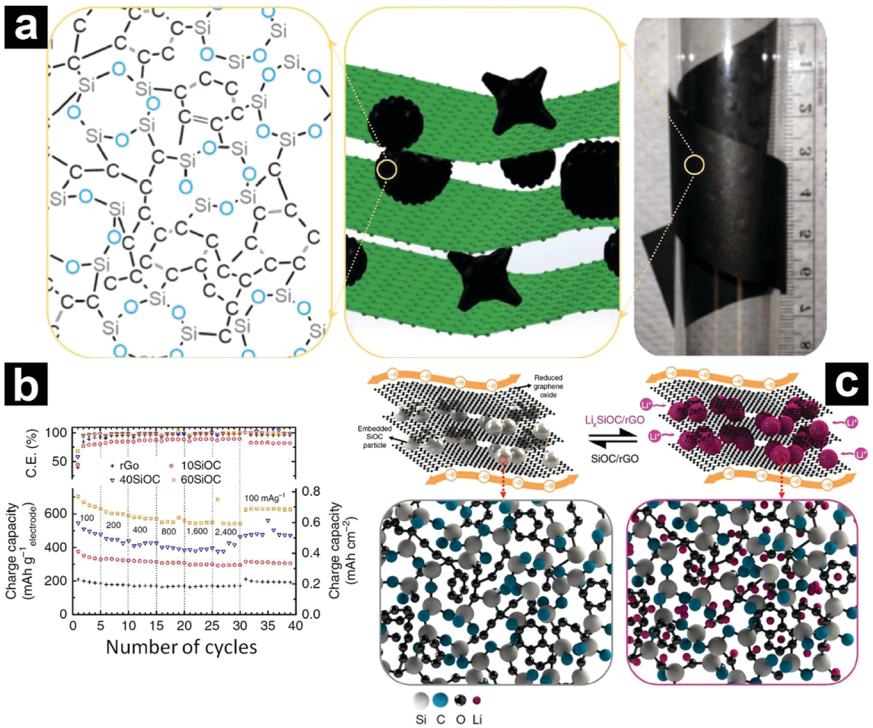

Fig. 21 Digital photo, schematic illustration of the free-standing SiOC/rGO composite, and the atomic structure of SiOC (a); rate performance of SiOC/rGO composites with different SiOC contents (b), and schematic illustration showing the lithiation/de-lithiation mechanism of SiOC/rGO composites (c). Reproduced with permission from ref. 213. Copyright 2016, Nature Publishing Group.

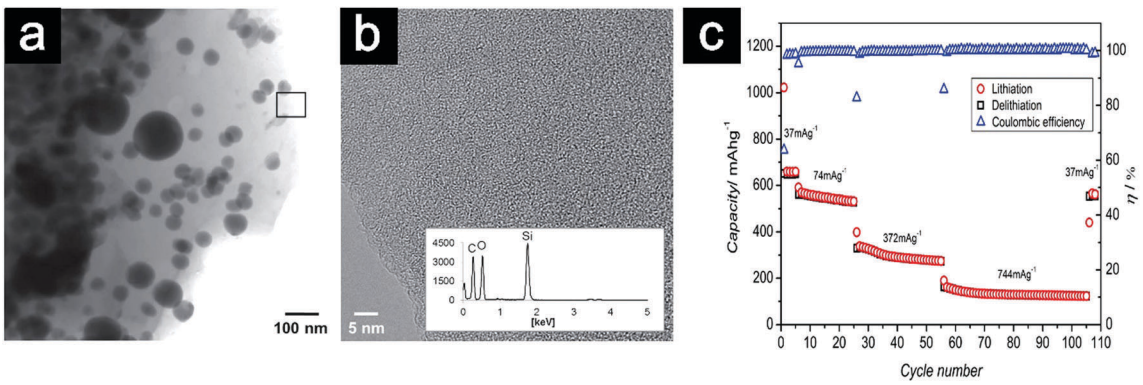

Fig. 22 TEM image of SiOC/Sn (a); high-resolution image with EDS pattern of the amorphous SiOC matrix (b); rate performance and coulombic efficiency (η) of SiOC/Sn (c). Reproduced with permission from ref. 243. Copyright 2014, Wiley-VCH.

filtration (Fig. 21a).[213] The obtained free-standing electrode (60SiOC with a SiOC content of 65–78 wt%) afforded a specific capacity of 702 mA h g^{-1} at 100 mA g^{-1}, retaining 543 mA h g^{-1} at 2400 mA g^{-1} (Fig. 21b). In addition, after cycling at 1600 mA g^{-1} for 1010 cycles, a capacity of 588 mA h g^{-1} can be recovered after reducing the current density to 100 mA g^{-1}. In the composite electrode, the SiOC particles acted as the major active component for lithium storage, while the rGO served as the electron conductor as well as the current collector (Fig. 20c).

5.2.3 SiOC/metal hybrid anode materials. Introducing metal into SiOC to prepare SiOC/metal hybrid anodes has also been regarded as an effective approach to realize further improvement in the electrochemical performance. Kaspar *et al.* prepared SiOC/Sn nanocomposites through chemical modification of polysiloxane Polyramic RD-684a (SiOC) with tin(II) acetate, and then annealing at 1000 °C. The obtained SiOC/Sn exhibited a capacity of 562 mA h g^{-1} at 74 mA g^{-1} with little fading after 20 cycles. Even at a high current density of 744 mA g^{-1}, a significant electrochemical activity (133 mA h g^{-1}) can still be detected (Fig. 22a–c).[243]

6. Conclusions

Silicon oxide-based materials, including SiO, SiO_2, SiO_x, and SiOC, represent an attractive family of high-capacity anode

materials for next-generation LIBs. The issues facing such materials include the low intrinsic electrical conductivity, drastic volume fluctuation during lithiation/de-lithiation, and low ICE. This Review presents a comprehensive summary on the most important progress in the microstructure, lithium storage mechanism, synthesis, and electrochemical properties of silicon oxide-based anode materials. Particular emphasis has been placed on tackling the remaining issues of silicon oxide-based anode materials through rational structural design, such as constructing unique nanostructures, fabricating silicon oxide/carbon hybrids, and designing silicon oxide/metal composites. Other strategies for electrochemical performance enhancement, such as controlled pre-lithiation and polymer binder optimization has also been covered.

Despite the tremendous efforts, the development of silicon oxide-based anode materials is still in its infancy. There is a long way to go before large-scale practical application. Among the various silicon oxide-based anode materials, the SiO and Si-rich SiO_x are relatively close to commercialization. Their volume change can be alleviated through delicate structure optimization and a stable cycling of over hundreds of cycles can be achieved. However, the ICE and average coulombic efficiency during cycling remain relatively low. For SiO_2, O-rich SiO_x, and SiOC, they display excellent cycling stability after proper structure design; however, they also suffer from the coulombic efficiency issue. In addition, the large voltage hysteresis (the difference in charge and discharge voltages) hinders their practical applications.

As for the future research on silicon oxide-based anode materials, we believe that it should be devoted to the following aspects:

(i) Feasible, scalable, and controlled pre-lithiation technologies should be developed to improve the ICE of silicon oxide-based anode materials. The ICE of bare silicon oxides is only 50–60%. Even for carbon coated silicon oxides, it is challenging to achieve an ICE value of over 80%. For practical applications in full cells, an ICE value of above 85% is required.

(ii) The O content of silicon oxides should be optimized to achieve high specific capacity, extended cycle life, and low voltage hysteresis (high energy efficiency). The O content plays a significant role in the lithium storage performances of silicon oxides. The difficulty in achieving extended cycle life and low voltage hysteresis simultaneously is that they require contradictory material features. The extended cycle life requires a high O content (more Li_2O and lithium silicates) for volume change accommodation. However, a high O content usually leads to high voltage hysteresis.

(iii) Effective and controllable reduction methods for converting SiO_2 to SiO_x should be developed. Generally speaking, SiO_x with a relatively low O content (including SiO) is required in LIB technology. However, Si mainly exists as Si(IV), that is to say, SiO_2 and silicates, in nature. This situation necessitates cost-effective reduction methods.

(iv) The reaction mechanism between Li and silicon oxides should be better understood. There is still debate on the reaction pathways and final products. Deepening the basic understanding of the reaction mechanism would help in designing better silicon oxide-based anode materials.

(v) Novel binders and electrolyte additives suitable for high-capacity silicon oxide-based anode materials should be explored. The large volume variation of silicon oxides during cycling would lead to electrode disintegration and SEI film rupture. Novel binders and electrolyte additives which can improve electrode integrity and SEI film stability are worth exploring.

With continuous and intensive worldwide efforts, we believe that breakthroughs will no doubt be made in silicon oxide-based anode materials in the near future. And we are confident that the silicon oxide-based anode materials will play an increasingly important and active role in next-generation high-energy density LIBs.

Conflicts of interest

There are no conflicts to declare.

Acknowledgements

This work was supported by the National Key R&D Program of China (2018YFB0104200).

Notes and references

1 M. Armand and J. M. Tarascon, *Nature*, 2008, **451**, 652–657.
2 J. W. Choi and D. Aurbach, *Nat. Rev. Mater.*, 2016, **1**, 16013.
3 R. F. Service, *Science*, 2014, **344**, 352–354.
4 J. M. Tarascon and M. Armand, *Nature*, 2001, **414**, 359–367.
5 M. S. Whittingham, *Chem. Rev.*, 2004, **35**, 4271–4301.
6 M. Pasta, C. D. Wessells, R. A. Huggins and Y. Cui, *Nat. Commun.*, 2012, **3**, 1149.
7 Y. Idota, T. Kubota, A. Matsufuji, Y. Maekawa and T. Miyasaka, *Science*, 1997, **276**, 1395–1397.
8 J. Maier, *Nat. Mater.*, 2005, **4**, 805–815.
9 J. R. Owen, *Chem. Soc. Rev.*, 1997, **26**, 259–267.
10 R. Yazami and P. Touzain, *J. Power Sources*, 1983, **9**, 365–371.
11 K. Zaghib, M. Simoneau, M. Armand and M. Gauthier, *J. Power Sources*, 1999, **81**, 300–305.
12 C. Zhang, N. Mahmood, H. Yin, F. Liu and Y. Hou, *Adv. Mater.*, 2013, **25**, 4932–4937.
13 L. Wang, X. He, J. Li, W. Sun, J. Gao, J. Guo and C. Jiang, *Angew. Chem., Int. Ed.*, 2012, **51**, 9034–9037.
14 K. T. Lee, Y. S. Jung and S. M. Oh, *J. Am. Chem. Soc.*, 2003, **125**, 5652–5653.
15 W. M. Zhang, J. S. Hu, Y. G. Guo, S. F. Zheng, L. S. Zhong, W. G. Song and L. J. Wan, *Adv. Mater.*, 2010, **20**, 1160–1165.
16 P. V. Prikhodchenko, J. Gun, S. Sladkevich, A. A. Mikhaylov, O. Lev, Y. Y. Tay, S. K. Batabyal and D. Y. W. Yu, *Chem. Mater.*, 2012, **24**, 4750–4757.
17 W. Luo, P. Zhang, X. Wang, Q. Li, Y. Dong, J. Hua, L. Zhou and L. Mai, *J. Power Sources*, 2016, **304**, 340–345.
18 S. Choi, Y. G. Cho, J. Kim, N. S. Choi, H. K. Song, G. Wang and S. Park, *Small*, 2017, **13**, 1603045.
19 C. K. Chan, X. F. Zhang and Y. Cui, *Nano Lett.*, 2008, **8**, 307–309.

20 H. Jia, R. Kloepsch, X. He, J. P. Badillo, P. Gao, O. Fromm, T. Placke and M. Winter, *Chem. Mater.*, 2015, **26**, 5683–5688.
21 X. Li, Z. Yang, Y. Fu, L. Qiao, D. Li, H. Yue and D. He, *ACS Nano*, 2015, **9**, 1858–1867.
22 D. J. Xue, S. Xin, Y. Yan, K. C. Jiang, Y. X. Yin, Y. G. Guo and L. J. Wan, *J. Am. Chem. Soc.*, 2012, **134**, 2512–2515.
23 P. Poizot, S. Laruelle, S. Grugeon, L. Dupont and J. M. Tarascon, *Nature*, 2000, **407**, 496–499.
24 M. V. Reddy, G. V. Subba Rao and B. V. Chowdari, *Chem. Rev.*, 2013, **113**, 5364–5457.
25 J. Cabana, L. Monconduit, D. Larcher and M. R. Palacin, *Adv. Mater.*, 2010, **22**, E170–E192.
26 H. Kim, B. Han, J. Choo and J. Cho, *Angew. Chem., Int. Ed.*, 2008, **47**, 10151–10154.
27 A. Magasinski, P. Dixon, B. Hertzberg, A. Kvit, J. Ayala and G. Yushin, *Nat. Mater.*, 2010, **9**, 353–358.
28 J. Liu, P. Kopold, P. A. Van Aken, J. Maier and Y. Yu, *Angew. Chem., Int. Ed.*, 2015, **54**, 9632–9636.
29 C. K. Chan, H. Peng, G. Liu, K. Mcilwrath, X. F. Zhang, R. A. Huggins and Y. Cui, *Nat. Nanotechnol.*, 2008, **3**, 31.
30 S. W. Lee, M. T. Mcdowell, J. W. Choi and Y. Cui, *Nano Lett.*, 2011, **11**, 3034.
31 C. Wang, H. Wu, Z. Chen, M. T. Mcdowell, Y. Cui and Z. Bao, *Nat. Chem.*, 2013, **5**, 1042.
32 D. Lin, Z. Lu, P. C. Hsu, H. R. Lee, N. Liu, J. Zhao, H. Wang, C. Liu and Y. Cui, *Energy Environ. Sci.*, 2015, **8**, 2371–2376.
33 T. Chen, J. Wu, Q. Zhang and X. Su, *J. Power Sources*, 2017, **363**, 126–144.
34 J. Y. Li, Q. Xu, G. Li, Y. X. Yin, L. J. Wan and Y. G. Guo, *Mater. Chem. Front.*, 2017, **1**, 1691–1708.
35 H. K. Liu, Z. P. Guo, J. Z. Wang and K. Konstantinov, *J. Mater. Chem.*, 2010, **20**, 10055–10057.
36 H. Kim, E. J. Lee and Y. K. Sun, *Mater. Today*, 2014, **17**, 285–297.
37 A. R. Kamali and D. J. Fray, *J. New Mater. Electrochem. Syst.*, 2010, **13**, 147–160.
38 C. F. Mabery, *Am. Chem. J.*, 1887, **9**, 11.
39 H. N. Potter, *Trans. Am. Electrochem. Soc.*, 1907, **12**, 191.
40 S. M. Schnurre, J. Grobner and R. Schmid-Fetzer, *J. Non-Cryst. Solids*, 2004, **336**, 1–25.
41 K. Alkaabi, D. L. Prasad, P. Kroll, N. W. Ashcroft and R. Hoffmann, *J. Am. Chem. Soc.*, 2014, **136**, 3410–3423.
42 H. R. Philipp, *J. Phys. Chem. Solids*, 1971, **32**, 1935–1945.
43 H. R. Philipp, *J. Non-Cryst. Solids*, 1972, **8**, 627–632.
44 G. W. Brady, *J. Phys. Chem.*, 1959, **63**, 199–202.
45 R. J. Temkin, *J. Non-Cryst. Solids*, 1975, **17**, 215–230.
46 F. Ekkehard and U. Schubert, *Chem. Mater.*, 1999, **11**, 865–866.
47 A. Hohl, T. Wieder, P. A. V. Aken, T. E. Weirich, G. Denninger, M. Vidal, S. Oswald, C. Deneke, J. Mayer and H. Fuess, *J. Non-Cryst. Solids*, 2003, **320**, 255–280.
48 K. Schulmeister and W. Mader, *J. Non-Cryst. Solids*, 2003, **320**, 143–150.
49 A. Hirata, S. Kohara, T. Asada, M. Arao, C. Yogi, H. Imai, Y. Tan, T. Fujita and M. Chen, *Nat. Commun.*, 2016, **7**, 11591.
50 G. Hass, *J. Am. Ceram. Soc.*, 1950, **33**, 353–360.
51 M. Mamiya, H. Takei, M. Kikuchi and C. Uyeda, *J. Cryst. Growth*, 2001, **229**, 457–461.
52 M. Mamiya, M. Kikuchi and H. Takei, *J. Cryst. Growth*, 2002, **237**, 1909–1914.
53 Y. Idota, Y. Mineo, A. Matsufuji and T. Miyasaki, *Denki Kagaku*, 1997, **65**, 717.
54 K. Tahara, H. Ishikawa, F. Iwasaki, S. Yahagi, A. Sakata and T. Sakai, *European Pat.*, 0582173 A1, 1993; K. Tahara, H. Ishikawa, F. Iwasaki, S. Yahagi, A. Sakata and T. Sakai, *European Pat.*, 582173 A1 93111938.2, 1994.
55 K. Tahara, F. Iwasaki, T. Tamachi and T. Sakai, *38th Battery Symposium in Japan, Abstr.*, 1997, 179–180.
56 H. Morimoto, M. Tatsumisago and T. Minami, *Electrochem. Solid-State Lett.*, 2001, **4**, A16–A18.
57 J. Yang, Y. Takeda, N. Imanishi, C. Capiglia, J. Y. Xie and O. Yamamoto, *Solid State Ionics*, 2002, **152**, 125–129.
58 A. Netz, R. A. Huggins and W. Weppner, *J. Power Sources*, 2003, **119**, 95–100.
59 Y. Liu, K. Hanai, J. Yang, N. Imanishi, A. Hirano and Y. Takeda, *Solid State Ionics*, 2004, **168**, 61–68.
60 A. Netz and R. A. Huggins, *Solid State Ionics*, 2004, **175**, 215–219.
61 H. Y. Lee and S. M. Lee, *Electrochem. Commun.*, 2004, **6**, 465–469.
62 T. Morita and N. Takami, *J. Electrochem. Soc.*, 2006, **153**, A425–A430.
63 X. Yang, Z. Wen, X. Xu, B. Lin and S. Huang, *J. Power Sources*, 2007, **164**, 880–884.
64 T. Zhang, J. Gao, H. P. Zhang, L. C. Yang, Y. P. Wu and H. Q. Wu, *Electrochem. Commun.*, 2007, **9**, 886–890.
65 G. Jeong, Y. U. Kim, S. A. Krachkovskiy and C. K. Lee, *Chem. Mater.*, 2010, **22**, 5570–5579.
66 X. Yuan, Y. J. Chao, Z. F. Ma and X. Deng, *Electrochem. Commun.*, 2007, **9**, 2591–2595.
67 Y. Nagao, H. Sakaguchi, H. Honda, T. Fukunaga and T. Esaka, *J. Electrochem. Soc.*, 2004, **151**, A1572–A1575.
68 M. Mariko, Y. Hironori, K. Hidemasa, O. Tomoyuki and S. Masato, *J. Electrochem. Soc.*, 2005, **152**, A2089–A2091.
69 T. Kim, S. Park and S. M. Oh, *J. Electrochem. Soc.*, 2007, **154**, A1112–A1117.
70 J. H. Kim, C. M. Park, H. Kim, Y. J. Kim and H. J. Sohn, *J. Electroanal. Chem.*, 2011, **661**, 245–249.
71 M. Yamada, A. Inaba, A. Ueda, K. Matsumoto, T. Iwasaki and T. Ohzuku, *J. Electrochem. Soc.*, 2012, **159**, A1630–A1635.
72 Y. Hwa, C. M. Park and H. J. Sohn, *J. Power Sources*, 2013, **222**, 129–134.
73 T. Kajita, R. Yuge, K. Nakahara, J. Iriyama, H. Takahashi, R. Kasahara, T. Numata, S. Serizawa and K. Utsugi, *J. Electrochem. Soc.*, 2013, **160**, A1806–A1810.
74 B. C. Yu, Y. Hwa, C. M. Park and H. J. Sohn, *J. Mater. Chem. A*, 2013, **1**, 4820–4825.
75 J. K. Lee, W. Y. Yoon and B. K. Kim, *J. Electrochem. Soc.*, 2014, **161**, A927–A933.
76 B. C. Yu, Y. Hwa, J. H. Kim and H. J. Sohn, *Electrochim. Acta*, 2014, **117**, 426–430.
77 S. C. Jung, H. J. Kim, J. H. Kim and Y. K. Han, *J. Phys. Chem. C*, 2015, **120**, 886–892.

78 M. Miyachi, H. Yamamoto and H. Kawai, *J. Electrochem. Soc.*, 2007, **154**, A376–A380.
79 S. Komaba, K. Shimomura, N. Yabuuchi, T. Ozeki, H. Yui and K. Konno, *J. Phys. Chem. C*, 2011, **115**, 13487–13495.
80 X. Feng, J. Yang, X. Yu, J. Wang and Y. Nuli, *J. Solid State Electrochem.*, 2013, **17**, 2461–2469.
81 H. Wu, G. Chan, J. W. Choi, I. Ryu, Y. Yao, M. T. Mcdowell, S. W. Lee, A. Jackson, Y. Yang and L. Hu, *Nat. Nanotechnol.*, 2012, **7**, 310–315.
82 J. H. Kim, H. J. Sohn, H. Kim, G. Jeong and W. Choi, *J. Power Sources*, 2007, **170**, 456–459.
83 C. H. Doh, C. W. Park, H. M. Shin, D. H. Kim, Y. D. Chung, S. I. Moon, B. S. Jin, H. S. Kim and A. Veluchamy, *J. Power Sources*, 2008, **179**, 367–370.
84 H. Zhao, Z. Wang, P. Lu, M. Jiang, F. Shi, X. Song, Z. Zheng, X. Zhou, Y. Fu and G. Abdelbast, *Nano Lett.*, 2015, **14**, 6704–6710.
85 H. Zhao, N. Yuca, Z. Zheng, Y. Fu, V. S. Battaglia, G. Abdelbast, K. Zaghib and G. Liu, *ACS Appl. Mater. Interfaces*, 2015, **7**, 862–866.
86 Y. Kobayashi, S. Seki, Y. Mita, Y. Ohno, H. Miyashiro, P. Charest, A. Guerfi and K. Zaghib, *J. Power Sources*, 2008, **185**, 542–548.
87 M. Yamada, A. Ueda, K. Matsumoto and T. Ohzuku, *J. Electrochem. Soc.*, 2011, **158**, A417–A421.
88 Y. Ren, J. Ding, N. Yuan, S. jia, M. Qu and Z. Yu, *J. Solid State Electrochem.*, 2012, **16**, 1453–1460.
89 I. Choi, J. L. Min, S. M. Oh and J. J. Kim, *Electrochim. Acta*, 2012, **85**, 369–376.
90 K. W. Kim, H. Park, J. G. Lee, J. Kim, Y. U. Kim, H. R. Ji, J. J. Kim and S. M. Oh, *Electrochim. Acta*, 2013, **103**, 226–230.
91 J. L. Dong, M. H. Ryou, J. N. Lee, B. G. Kim, M. L. Yong, H. W. Kim, B. S. Kong, J. K. Park and J. W. Choi, *Electrochem. Commun.*, 2013, **34**, 98–101.
92 M. J. Jung, K. Y. Sheem and Y. S. Lee, *J. Nanosci. Nanotechnol.*, 2014, **14**, 2852–2858.
93 M. Yamada, K. Uchitomi, A. Ueda, K. Matsumoto and T. Ohzuku, *J. Power Sources*, 2013, **225**, 221–225.
94 L. Shi, C. Pang, S. Chen, M. Wang, K. Wang, Z. Tan, P. Gao, J. Ren, Y. Huang and H. Peng, *Nano Lett.*, 2017, **17**, 3681.
95 C. M. Park, W. Choi, Y. Hwa, J. H. Kim, G. Jeong and H. J. Sohn, *J. Mater. Chem.*, 2010, **20**, 4854–4860.
96 Q. Si, K. Hanai, T. Ichikawa, M. B. Phillipps, A. Hirano, N. Imanishi, O. Yamamoto and Y. Takeda, *J. Power Sources*, 2011, **196**, 9774–9779.
97 C. Guo, D. Wang, Q. Wang, B. Wang and T. Liu, *Int. J. Electrochem. Sci.*, 2012, **7**, 8745–8752.
98 W. R. Liu, Y. C. Yen, H. C. Wu, M. Winter and N. L. Wu, *J. Appl. Electrochem.*, 2009, **39**, 1643–1649.
99 J. I. Lee and S. Park, *Nano Energy*, 2013, **2**, 146–152.
100 J. I. Lee, K. T. Lee, J. Cho, J. Kim, N. S. Choi and S. Park, *Angew. Chem., Int. Ed.*, 2012, **124**, 2767–2771.
101 G. Jeong, J. H. Kim, Y. U. Kim and Y. J. Kim, *J. Mater. Chem.*, 2012, **22**, 7999–8004.
102 H. Morimoto, T. Sudo, H. Watanabe and S. I. Tobishima, *Electrochemistry*, 2012, **80**, 812–816.
103 M. Zhou, M. L. Gordin, S. Chen, T. Xu, J. Song, D. Lv and D. Wang, *Electrochem. Commun.*, 2013, **28**, 79–82.
104 B. Liu, A. Abouimrane, Y. Ren, M. Balasubramanian, D. Wang, Z. Z. Fang and K. Amine, *Chem. Mater.*, 2012, **24**, 4653–4661.
105 B. Liu, A. Abouimrane, D. Brown, X. Zhang, Y. Ren, Z. Fang and K. Amine, *J. Mater. Chem. A*, 2013, **1**, 4376–4382.
106 H. Zhao, Q. Yang, N. Yuca, M. Ling, K. Higa, V. S. Battaglia, D. Y. Parkinson, V. Srinivasan and G. Liu, *Nano Lett.*, 2016, **16**, 4686.
107 X. Wang, Z. Wen, L. Yu and X. Wu, *Electrochim. Acta*, 2009, **54**, 4662–4667.
108 X. Wang, Z. Wen, Y. Liu, Y. Huang and T. L. Wen, *Solid State Ionics*, 2011, **192**, 330–334.
109 I. W. Seong, K. T. Kim, W. Y. Yoon, I. W. Seong, K. T. Kim and W. Y. Yoon, *J. Power Sources*, 2009, **189**, 511–514.
110 I. W. Seong and W. Y. Yoon, *J. Power Sources*, 2010, **195**, 6143–6147.
111 J. H. Yom, W. H. Sun, S. M. Cho and W. Y. Yoon, *J. Power Sources*, 2016, **311**, 159–166.
112 H. J. Kim, S. Choi, S. J. Lee, M. W. Seo, J. G. Lee, E. Deniz, J. L. Yong, E. K. Kim and J. W. Choi, *Nano Lett.*, 2016, **16**, 282.
113 H. Yamamura, S. Nakanishi and H. Iba, *J. Power Sources*, 2013, **232**, 264–269.
114 M. J. Schultz and M. S. Sigman, *J. Am. Chem. Soc.*, 2006, **128**, 1460.
115 Z. Bao, M. R. Weatherspoon, S. Shian, Y. Cai, P. D. Graham, S. M. Allan, G. Ahmad, M. B. Dickerson, B. C. Church and Z. Kang, *Nature*, 2007, **38**, 172–175.
116 N. Liu, K. Huo, M. T. Mcdowell, J. Zhao and Y. Cui, *Sci. Rep.*, 2013, **3**, 1919.
117 A. Lisowska-Oleksiak, A. P. Nowak and B. Wicikowska, *RSC Adv.*, 2014, **4**, 40439–40443.
118 J. Liu, P. Kopold, P. A. Van Aken, J. Maier and Y. Yu, *Angew. Chem., Int. Ed.*, 2015, **127**, 9632–9636.
119 J. Cui, Y. Cui, S. Li, H. Sun, Z. Wen and J. Sun, *ACS Appl. Mater. Interfaces*, 2016, **8**, 30239.
120 Y. Ju, J. A. Tang, K. Zhu, Y. Meng, C. Wang, G. Chen, Y. Wei and Y. Gao, *Electrochim. Acta*, 2016, **191**, 411–416.
121 Y. Shen, *J. Agric. Food Chem.*, 2017, **65**, 995.
122 J. Cui, F. Cheng, J. Lin, J. Yang, K. Jiang, Z. Wen and J. Sun, *Powder Technol.*, 2017, **311**, 1–8.
123 H. Huang, E. M. Kelder, L. Chen and J. Schoonman, *J. Power Sources*, 1999, **81**, 362–367.
124 B. Gao, S. Sinha, L. Fleming and O. Zhou, *Adv. Mater.*, 2001, **13**, 816–819.
125 B. Guo, J. Shu, Z. Wang, H. Yang, L. Shi, Y. Liu and L. Chen, *Electrochem. Commun.*, 2008, **10**, 1876–1878.
126 Q. Sun, B. Zhang and Z.-W. Fu, *Appl. Surf. Sci.*, 2008, **254**, 3774–3779.
127 C. Ban, B. B. Kappes, Q. Xu, C. Engtrakul, C. V. Ciobanu, A. C. Dillon and Y. Zhao, *Appl. Phys. Lett.*, 2012, **100**, 243905.
128 Y. Zhang, Y. Li, Z. Wang and K. Zhao, *Nano Lett.*, 2014, **14**, 7161–7170.
129 S. Perez-Beltran, G. E. Ramírez-Caballero and P. B. Balbuena, *J. Phys. Chem. C*, 2015, **119**, 16424–16431.

130 A. Ostadhossein, S. Y. Kim, E. D. Cubuk, Y. Qi and A. C. van Duin, *J. Phys. Chem. A*, 2016, **120**, 2114–2127.
131 G. Lener, M. Otero, D. E. Barraco and E. P. M. Leiva, *Electrochim. Acta*, 2018, **259**, 1053–1058.
132 G. Lener, A. A. Garcia-Blanco, O. Furlong, M. Nazzarro, K. Sapag, D. E. Barraco and E. P. M. Leiva, *Electrochim. Acta*, 2018, **279**, 289–300.
133 Y. G. Guo, J. S. Hu and L. J. Wan, *Adv. Mater.*, 2008, **20**, 2878–2887.
134 P. G. Bruce, B. Scrosati and J. M. Tarascon, *Angew. Chem., Int. Ed.*, 2008, **47**, 2930–2946.
135 Y. Zhong, M. Yang, X. Zhou and Z. Zhou, *Mater. Horiz.*, 2015, **2**, 553–566.
136 Y. Sun, N. Liu and Y. Cui, *Nat. Energy*, 2016, **1**, 16071.
137 J. Tu, Y. Yuan, P. Zhan, H. Jiao, X. Wang, H. Zhu and S. Jiao, *J. Phys. Chem. C*, 2014, **118**, 7357–7362.
138 C. Liang, L. Zhou, C. Zhou, H. Huang, S. Liang, Y. Xia, Y. Gan, X. Tao, J. Zhang and W. Zhang, *Mater. Res. Bull.*, 2017, **96**, 347–353.
139 W. S. Chang, C. M. Park, J. H. Kim, Y. U. Kim, G. Jeong and H. J. Sohn, *Energy Environ. Sci.*, 2012, **5**, 6895–6899.
140 X. W. Lou, L. A. Archer and Z. Yang, *Adv. Mater.*, 2008, **20**, 3987–4019.
141 Z. Wang, Z. Liang and W. L. Xiong, *Adv. Mater.*, 2012, **24**, 1903–1911.
142 L. Zhou, Z. Zhuang, H. Zhao, M. Lin, D. Zhao and L. Mai, *Adv. Mater.*, 2017, **29**, 1602914.
143 M. Sasidharan, D. Liu, N. Gunawardhana, M. Yoshio and K. Nakashima, *J. Mater. Chem.*, 2011, **21**, 13881–13888.
144 M. Sasidharan, K. Nakashima, N. Gunawardhana, T. Yokoi, M. Ito, M. Inoue, S. Yusa, M. Yoshio and T. Tatsumi, *Nanoscale*, 2011, **3**, 4768–4773.
145 X. Ma, Z. Wei, H. Han, X. Wang, K. Cui and L. Yang, *Chem. Eng. J.*, 2017, **323**, 252–259.
146 N. Yan, F. Wang, H. Zhong, Y. Li, Y. Wang, L. Hu and Q. Chen, *Sci. Rep.*, 2013, **3**, 1568.
147 Z. Favors, W. Wang, H. H. Bay, A. George, M. Ozkan and C. S. Ozkan, *Sci. Rep.*, 2014, **4**, 4605.
148 Y. Yu, J. Zhang, L. Xue, T. Huang and A. Yu, *J. Power Sources*, 2011, **196**, 10240–10243.
149 X. Yang, H. Huang, Z. Li, M. Zhong, G. Zhang and D. Wu, *Carbon*, 2014, **77**, 275–280.
150 Y. Liang, L. Cai, L. Chen, X. Lin, R. Fu, M. Zhang and D. Wu, *Nanoscale*, 2015, **7**, 3971.
151 S. Hao, Z. Wang and L. Chen, *Mater. Des.*, 2016, **111**, 616–621.
152 C. Gao, H. Zhao, P. Lv, C. Wang, J. Wang, T. Zhang and Q. Xia, *J. Electrochem. Soc.*, 2014, **161**, A2216–A2221.
153 H.-H. Li, X.-L. Wu, H.-Z. Sun, K. Wang, C.-Y. Fan, L.-L. Zhang, F.-M. Yang and J.-P. Zhang, *J. Phys. Chem. C*, 2015, **119**, 3495–3501.
154 H. H. Li, L. L. Zhang, C. Y. Fan, K. Wang, X. L. Wu, H. Z. Sun and J. P. Zhang, *Phys. Chem. Chem. Phys.*, 2015, **17**, 22893–22899.
155 X. Cao, X. Chuan, R. C. Masse, D. Huang, S. Li and G. Cao, *J. Mater. Chem. A*, 2015, **3**, 22739–22749.
156 Y. K. Kim, J. W. Moon, J. G. Lee, Y. K. Baek and S. H. Hong, *J. Power Sources*, 2014, **272**, 689–695.
157 W. An, J. Fu, J. Su, L. Wang, X. Peng, K. Wu, Q. Chen, Y. Bi, B. Gao and X. Zhang, *J. Power Sources*, 2017, **345**, 227–236.
158 H. Wang, P. Wu, M. Qu, L. Si, Y. Tang, Y. Zhou and T. Lu, *ChemElectroChem*, 2015, **2**, 508–511.
159 J. Y. Kim, T. N. Dan, J. S. Kang and S. W. Song, *J. Alloys Compd.*, 2015, **633**, 92–96.
160 X. Liu, Y. Chen, H. Liu and Z. Q. Liu, *J. Mater. Sci. Technol.*, 2017, **33**, 239–245.
161 M. Jiao, K. Liu, Z. Shi and C. Wang, *ChemElectroChem*, 2017, **4**, 542–549.
162 D. Nan, J. G. Wang, Z. H. Huang, L. Wang, W. Shen and F. Kang, *Electrochem. Commun.*, 2013, **34**, 52–55.
163 X. Wu, Z. Q. Shi, C. Y. Wang and J. Jin, *J. Electroanal. Chem.*, 2015, **746**, 62–67.
164 M. Li, Y. Yu, J. Li, B. Chen, X. Wu, Y. Tian and P. Chen, *J. Mater. Chem. A*, 2015, **3**, 1476–1482.
165 J. Meng, Y. Cao, Y. Suo, Y. Liu, J. Zhang and X. Zheng, *Electrochim. Acta*, 2015, **176**, 1001–1009.
166 Z. Xiang, Y. Chen, J. Li, X. Xia, Y. He and H. Liu, *J. Solid State Electrochem.*, 2017, **21**, 2425–2432.
167 Y. Yuan, S. Wang, Z. Kang and S. Jiao, *Electrochemistry*, 2015, **83**, 421–424.
168 A. Molkenova and I. Taniguchi, *Adv. Powder Technol.*, 2015, **26**, 377–384.
169 H. Gong, N. Li and Y. Qian, *Int. J. Electrochem. Sci.*, 2013, **8**, 9811–9817.
170 Y. Ren, H. Wei, X. Huang and J. Ding, *Int. J. Electrochem. Sci.*, 2014, **9**, 7784–7794.
171 P. Lv, H. Zhao, J. Wang, X. Liu, T. Zhang and Q. Xia, *J. Power Sources*, 2013, **237**, 291–294.
172 D. Jia, K. Wang and J. Huang, *Chem. Eng. J.*, 2017, **317**, 673–686.
173 M. Li, Y. Yu, J. Li, B. Chen, X. Wu, Y. Tian and P. Chen, *J. Mater. Chem. A*, 2014, **3**, 1476–1482.
174 C. Tang, Y. Liu, C. Xu, J. Zhu, X. Wei, L. Zhou, L. He, W. Yang and L. Mai, *Adv. Funct. Mater.*, 2017, **28**, 1704561.
175 M. Li, J. Li, K. Li, Y. Zhao, Y. Zhang, D. Gosselink and P. Chen, *J. Power Sources*, 2013, **240**, 659–666.
176 H. Wang, X. Yang, Q. Wu, Q. Zhang, H. Chen, H. Jing, J. Wang, S. B. Mi, A. L. Rogach and C. Niu, *ACS Nano*, 2018, **12**, 3406–3416.
177 C. Y. Chou and G. S. Hwang, *Chem. Mater.*, 2013, **25**, 3435–3440.
178 F. G. B. Ooms, M. Wagemaker, A. A. Van Well, F. M. Mulder, E. M. Kelder and J. Schoonman, *Solid State Ionics*, 2002, **152**, 143–153.
179 K. Kim, J. H. Park, S. G. Doo and T. Kim, *Thin Solid Films*, 2010, **518**, 6547–6549.
180 P. R. Abel, Y. M. Lin, H. Celio, A. Heller and C. B. Mullins, *ACS Nano*, 2012, **6**, 2506.
181 S. W. Song, *J. Electrochem. Soc.*, 2013, **160**, A906–A914.
182 M. A. Al-Maghrabi, J. Suzuki, R. J. Sanderson, V. L. Chevrier, R. A. Dunlap and J. R. Dahn, *J. Electrochem. Soc.*, 2013, **160**, A1587–A1593.

183 K. K. Min, Y. J. Bo, S. L. Jin, J. S. Kim and S. Nahm, *J. Power Sources*, 2013, **244**, 115–121.
184 H. Takezawa, K. Iwamoto, S. Ito and H. Yoshizawa, *J. Power Sources*, 2013, **244**, 149–157.
185 S. S. Suh, W. Y. Yoon, D. H. Kim, S. U. Kwon, J. H. Kim, Y. U. Kim, C. U. Jeong, Y. Y. Chan, S. H. Kang and J. K. Lee, *Electrochim. Acta*, 2014, **148**, 111–117.
186 C. Yang, Y. L. Zhang, J. H. Zhou, C. F. Lin, F. Lv, K. Wang, J. R. Feng, Z. K. Xu, J. B. Li and S. J. Guo, *J. Mater. Chem. A*, 2018, **6**, 8039–8046.
187 L. Zhang, J. Deng, L. Liu, W. Si, S. Oswald, L. Xi, M. Kundu, G. Ma, T. Gemming and S. Baunack, *Adv. Mater.*, 2014, **26**, 4527–4532.
188 M. Li, Y. Zeng, Y. Ren, C. Zeng, J. Gu, X. Feng and H. He, *J. Power Sources*, 2015, **288**, 53–61.
189 M. Li, Y. Yu, J. Li, B. Chen, A. Konarov and P. Chen, *J. Power Sources*, 2015, **293**, 976–982.
190 Y. Ren and M. Li, *J. Power Sources*, 2016, **306**, 459–466.
191 J. Wang, H. Zhao, J. He, C. Wang and J. Wang, *J. Power Sources*, 2011, **196**, 4811–4815.
192 P. Lv, H. Zhao, C. Gao, T. Zhang and X. Liu, *Electrochim. Acta*, 2015, **152**, 345–351.
193 P. Lv, H. Zhao, C. Gao, Z. Du, J. Wang and X. Liu, *J. Power Sources*, 2015, **274**, 542–550.
194 M. S. Park, E. Park, J. Lee, G. Jeong, K. J. Kim, J. H. Kim, Y. J. Kim and H. Kim, *ACS Appl. Mater. Interfaces*, 2014, **6**, 9608.
195 C. Guo, D. Wang, T. Liu, J. Zhu and X. Lang, *J. Mater. Chem. A*, 2014, **2**, 3521–3527.
196 Z. Liu, D. Guan, Q. Yu, L. Xu, Z. Zhuang, T. Zhu, D. Zhao, L. Zhou and L. Mai, *Energy Storage Mater.*, 2018, **13**, 112–118.
197 Z. H. Liu, Y. L. Zhao, R. H. He, W. Luo, J. S. Meng, Q. Yu, D. Y. Zhao, L. Zhou and L. Q. Mai, *Energy Storage Mater.*, 2018, DOI: 10.1016/j.ensm.2018.10.011.
198 Q. Xu, J. K. Sun, Y. X. Yin and Y. G. Guo, *Adv. Funct. Mater.*, 2018, **28**, 1705235.
199 Q. Xu, J. K. Sun, Z. L. Yu, Y. X. Yin, S. Xin, S. H. Yu and Y. G. Guo, *Adv. Mater.*, 2018, **30**, 1707430.
200 H. Zhang, R. Hu, Y. Liu, X. Cheng, J. Liu, Z. Lu, M. Zeng, L. Yang, J. Liu and M. Zhu, *Energy Storage Mater.*, 2018, **13**, 257–266.
201 K. Song, S. Yoo, K. Kang, H. Heo, Y. M. Kang and M. H. Jo, *J. Power Sources*, 2013, **229**, 229–233.
202 W. He, Y. Liang, H. Tian, S. Zhang, Z. Meng and W. Q. Han, *Energy Storage Mater.*, 2017, **8**, 119–126.
203 Y. Ren, X. Wu and M. Li, *Electrochim. Acta*, 2016, **206**, 328–336.
204 C. G. Pantano, A. K. Singh and H. Zhang, *J. Sol-Gel Sci. Technol.*, 1999, **14**, 7–25.
205 A. M. Wilson, J. N. Reimers, E. W. Fuller and J. R. Dahn, *Solid State Ionics*, 1994, **74**, 249–254.
206 A. M. Wilson, W. Xing, G. Zank, B. Yates and J. R. Dahn, *Solid State Ionics*, 1997, **100**, 259–266.
207 A. M. Wilson, G. Zank, K. Eguchi, W. Xing, B. Yates and J. R. Dahn, *Chem. Mater.*, 1997, **9**, 1601–1606.
208 A. M. Wilson, G. Zank, K. Eguchi, W. Xing and J. R. Dahn, *J. Power Sources*, 1997, **68**, 195–200.
209 W. Xing, A. M. Wilson, G. Zank and J. R. Dahn, *Solid State Ionics*, 1997, **93**, 239–244.
210 P. E. Sanchez-Jimenez and R. Raj, *J. Am. Ceram. Soc.*, 2010, **93**, 1127–1135.
211 J. Shen and R. Raj, *J. Power Sources*, 2011, **196**, 5945–5950.
212 X. Liu, M. C. Zheng and K. Xie, *J. Power Sources*, 2011, **196**, 10667–10672.
213 L. David, R. Bhandavat, U. Barrera and G. Singh, *Nat. Commun.*, 2016, **7**, 10998.
214 A. Saha, R. Raj and D. L. Williamson, *J. Am. Ceram. Soc.*, 2006, **89**, 2188–2195.
215 H. Fukui, H. Ohsuka, T. Hino and K. Kanamura, *ACS Appl. Mater. Interfaces*, 2010, **2**, 998–1008.
216 H. Fukui, N. Nakata, K. Dokko, B. Takemura, H. Ohsuka, T. Hino and K. Kanamura, *ACS Appl. Mater. Interfaces*, 2011, **3**, 2318.
217 X. Liu, K. Xie, C. M. Zheng, J. Wang and Z. Jing, *J. Power Sources*, 2012, **214**, 119–123.
218 N. Liao, B. Zheng, H. Zhou and W. Xue, *J. Mater. Chem. A*, 2015, **3**, 5067–5071.
219 V. S. Pradeep, M. Graczyk-Zajac, R. Riedel and G. D. Soraru, *Electrochim. Acta*, 2014, **119**, 78–85.
220 N. Liao, B. Zheng, H. Zhou and W. Xue, *Electrochim. Acta*, 2015, **156**, 115–120.
221 H. Konno, T. Kasashima and K. Azumi, *J. Power Sources*, 2009, **191**, 623–627.
222 M. Weinberger, C. Pfeifer, S. Schindler, T. Diemant, R. J. Behm and M. Wohlfahrtmehrens, *J. Mater. Chem. A*, 2015, **3**, 23707–23715.
223 G. Liu, J. Kaspar, L. M. Reinold, M. Graczyk-Zajac and R. Riedel, *Electrochim. Acta*, 2013, **106**, 101–108.
224 V. S. Pradeep, D. G. Ayana, M. Graczyk-Zajac, G. D. Soraru and R. Riedel, *Electrochim. Acta*, 2015, **157**, 41–45.
225 M. Halim, C. Hudaya, A. Kim and J. K. Lee, *J. Mater. Chem. A*, 2016, **4**, 2651–2656.
226 H. Shi, A. Yuan and J. Xu, *J. Power Sources*, 2017, **364**, 288–298.
227 H. Fukui, H. Ohsuka, T. Hino and K. Kanamura, *J. Electrochem. Soc.*, 2011, **158**, A550–A555.
228 M. S. Tahir, M. Weinberger, P. Balasubramanian, T. Diemant, R. J. Behm, M. Lindén and M. Wohlfahrt-Mehrens, *J. Mater. Chem. A*, 2017, **5**, 10190.
229 T. Momma, S. Aoki, H. Nara, T. Yokoshima and T. Osaka, *Electrochem. Commun.*, 2011, **13**, 969–972.
230 H. Nara, T. Yokoshima, T. Momma and T. Osaka, *Energy Environ. Sci.*, 2012, **5**, 6500–6505.
231 T. Hang, H. Nara and T. Yokoshima, *J. Power Sources*, 2013, **222**, 503–509.
232 T. Osaka, H. Nara, T. Momma and T. Yokoshima, *J. Mater. Chem. A*, 2014, **2**, 883–896.
233 T. Hang, D. Mukoyama, H. Nara, T. Yokoshima, T. Momma, M. Li and T. Osaka, *J. Power Sources*, 2014, **256**, 226–232.
234 S. Ahn, M. Jeong, T. Yokoshima, H. Nara, T. Momma and T. Osaka, *J. Power Sources*, 2016, **336**, 203–211.

235 H. Konno, T. Morishita, S. Sato, H. Habazaki, M. Inagaki, H. Konno, T. Morishita, S. Sato and M. Inagaki, *Carbon*, 2005, **43**, 1111–1114.
236 H. Konno, T. Morishita, C. Wan, T. Kasashima, H. Habazaki and M. Inagaki, *Carbon*, 2007, **45**, 477–483.
237 R. Bhandavat, M. Cologna and G. Singh, *Nanomater. Energy*, 2012, **1**, 57–61.
238 R. Bhandavat and G. Singh, *J. Phys. Chem. C*, 2013, **117**, 11899–11905.
239 Y. Li, Y. Hu, Y. Lu, S. Zhang, G. Xu, K. Fu, S. Li, C. Chen, L. Zhou and X. Xia, *J. Power Sources*, 2014, **254**, 33–38.
240 Y. R. Ren, B. Yang, X. B. Huang, F. Q. Chu, J. Qiu and J. N. Ding, *Solid State Ionics*, 2015, **278**, 198–202.
241 S. Ahn, M. Jeong, K. Miyamoto, T. Yokoshima, H. Nara, T. Momma and T. Osaka, *J. Electrochem. Soc.*, 2017, **164**, A355–A359.
242 Z. Y. Sang, Z. H. Zhao, D. Su, P. S. Miao, F. R. Zhang, H. M. Ji and X. Yan, *J. Mater. Chem. A*, 2018, **6**, 9064–9073.
243 J. Kaspar, C. Terzioglu, E. Ionescu, M. Graczyk-Zajac, S. Hapis, H. J. Kleebe and R. Riedel, *Adv. Funct. Mater.*, 2014, **24**, 4097–4104.